

# A STABILIZED MIXED FINITE ELEMENT APPROXIMATION FOR INCOMPRESSIBLE FINITE STRAIN SOLID DYNAMICS USING A TOTAL LAGRANGIAN FORMULATION

INOCENCIO CASTAÑAR<sup>§</sup>, JOAN BAIGES<sup>§</sup> AND RAMON CODINA<sup>§,‡</sup>

**ABSTRACT.** *In this work a new methodology for both the nearly and fully incompressible transient finite strain solid mechanics problem is presented. To this end, the momentum equation is complemented with a constitutive law for the pressure which emerges from the deviatoric/volumetric decomposition of the strain energy function for any hyperelastic material model. The incompressible limit is attained automatically depending on the material bulk modulus. The system is stabilized by means of the Variational Multiscale-Orthogonal Subgrid Scale method based on the decomposition of the unknowns into resolvable and subgrid scales in order to prevent pressure fluctuations. Several numerical examples are presented to assess the robustness and applicability of the proposed formulation.*

**Keywords:** Incompressible hyperelasticity, Solid dynamics, Mixed interpolations, Stabilization methods, Orthogonal subgrid scales.

## 1. INTRODUCTION

An incompressible material is understood as the one which keeps its volume constant throughout a motion. In many cases, this is a common idealization and accepted assumption often invoked in continuum and computational mechanics [1]. Numerous polymeric materials can sustain finite strains without noticeable volume changes. Furthermore, many biological materials and several types of soils can be modeled as nearly or fully incompressible [2].

Standard irreducible low order finite elements, in which only the displacement field is considered as the unknown variable of the problem and both stress and strain fields are obtained a posteriori, are typically preferred in complex engineering finite strain solid dynamics problems [3]. Nevertheless, this approach performs poorly in nearly and fully incompressible scenarios, producing solutions which are completely locked by the constraint. Volumetric and shear locking, pressure fluctuations and poor performance in bending dominated scenarios are some of the effects that we can observe in such situations [4].

Over the last years, different strategies and methodologies have been proposed to reduce or avoid these shortcomings by circumventing the inf-sup conditions (also called Ladyzhenskaya-Babuška-Brezzi (LBB) conditions) [5]. Reduced and selective integration techniques such as the B-bar, the F-bar or the well-known mean dilatation finite element method avoid these numerical instabilities by reducing the evaluations of the incompressibility constraints at quadrature points. Despite this, these strategies are only prepared to work with structured quadrilateral and structured hexahedral meshes. Many of these displacement-based methods have been shown to be equivalent to mixed methods in which

---

*Date:* November 18, 2019.

<sup>§</sup> Centre Internacional de Mètodes Numèrics en Enginyeria (CIMNE), Edifici C1, Campus Nord UPC, Gran Capitán S/N, 08034 Barcelona, Spain.

<sup>‡</sup> Universitat Politècnica de Catalunya, Barcelona Tech, Jordi Girona 1-3, Edifici C1, 08034 Barcelona, Spain.

E-mails: [icastanar@cimne.upc.edu](mailto:icastanar@cimne.upc.edu) (IC), [jbaiges@cimne.upc.edu](mailto:jbaiges@cimne.upc.edu) (JB), [ramon.codina@upc.edu](mailto:ramon.codina@upc.edu) (RC).

the stresses are approximated by fields of order lower than the displacements over the elements [6].

When considering the static, infinitesimal strain, incompressible case of the solid mechanics problem, we obtain an elliptic problem which is identical to the equations of the Stokes problem in fluid mechanics [7, 8]. For this reason, it makes sense to extend the mixed velocity/pressure pair used in the latter to the former for the mixed displacement/pressure approach [9]. This idea facilitated the extension of different implementations in the field of fluid mechanics to the solid mechanics area. See for instance [10, 11, 12], a set of works where the incompressible nonlinear material problem is stabilized using the orthogonal subscales method [13, 14], a variant of the stabilized method proposed in [15]. These works show the good performance of mixed finite elements using both strains/displacements and stresses/displacements pairs as primary variables. These formulations produce a considerable increase in the number of unknowns per node, but they also increase the accuracy for strains and stresses. Furthermore, in [16] the idea of using displacement/pressure/stress or displacement/pressure/strain formulations was tested and seen to be very effective when solving incompressible cases in which accurate results for stress and strain fields are required.

The majority of the previous works were developed for the static case. When considering the transient case, the elliptic problem becomes hyperbolic due to the second order derivative of the displacements which appears in the momentum equation. To the best of our knowledge, there exist two different effective methodologies in the literature to face this transient problem.

On the one hand, a new first-order mixed form of the equations of finite strain solid dynamics is presented in [17, 18, 19, 20]. In these works, the authors propose to use as primary variables the linear momentum  $\mathbf{p}$  and the deformation gradient  $\mathbf{F}$ . In order to effectively solve bending dominated scenarios in nearly incompressible cases they consider the introduction of the jacobian  $J$  as an extra unknown [21, 22, 23]. In more recent works [24, 25, 26], they insert the cofactor tensor of the deformation gradient  $\mathbf{H} = \text{cof } \mathbf{F}$  as an additional primary variable. The resulting system turns out to be unstable and for this reason, the authors stabilize the problem through a combination of the streamline upwind/Petrov Galerkin (SUPG) stabilization and different penalties on the deformation gradient. This methodology is very promising and it has been tested to be very effective to solve nearly incompressible cases. However, the number of unknowns per node increases drastically taking into account that both  $\mathbf{F}$  and  $\mathbf{H}$  are non-symmetric tensors.

On the other hand, an effective alternative taking the velocity/pressure pair as unknowns of the problem and updating the displacement explicitly as a final step was proposed in [27, 28]. The authors suggest to complement the momentum equation with a rate equation for the evolution of the pressure field and solve it by means of a two-step block Gauss-Seidel strategy, stabilized by means of the Variational Multi-Scale (VMS) method. This formulation is also very powerful despite the necessity of introducing the velocity field as a primary variable of the problem in addition to the pressure field.

In this paper we propose a novel way to solve the solid dynamics problem. Through the well-known deviatoric/volumetric decomposition of the strain energy [29] we complement the momentum equation in the context of the Total Lagrangian framework with the constitutive equation of the pressure. This equation is written so as to allow imposing the incompressibility constraint on hyperelastic materials naturally, introducing any change or additional equation in the system. The complete system which results from this formulation is unstable and it presents the well-known saddle-point structure. The resulting formulation will be stabilized by means of the VMS-Orthogonal SubGrid Scale (OSS) method, which is a stabilization technique well known for its low dissipative and highly accurate performance. The resulting method is very simple and only the addition of a scalar field as an extra primary variable is required.

This work is organized as follows: In Section 2 the solid dynamics equations are summarized as well as the constitutive equation of the additional pressure unknown. Furthermore, the variational form of the problem and the various employed time integrators are introduced. In Section 3 the OSS stabilization technique in hyperelastic models is presented and the stabilized form of the problem is shown. In Section 4 several benchmarks and numerical examples are tested to assess the present formulation and to validate its performance. To end up, in Section 5 some conclusions of the proposed formulation are drawn.

## 2. SOLID DYNAMICS PROBLEM

**2.1. Conservation equations.** In this work, the equations of motion of a body under finite strain assumption are considered. Let  $\Omega$  and  $\Omega_0$  be open, bounded and polyhedral domains of  $\mathbb{R}^d$ , where  $d \in \{2, 3\}$  is the number of space dimensions. The initial configuration of the body is denoted by  $\Omega_0$  whereas the current configuration of the body at time  $t$  is denoted by  $\Omega$ . Any point of the body in the reference configuration is labeled with the reference position vector  $\mathbf{X}$ . The components of the vector  $\mathbf{X}$  are considered as the material coordinates. On the other hand, the current position vector  $\mathbf{x}$  labels any point of the body at the deformed configuration. We assume the existence of a function  $\psi$  which characterises the motion:

$$\begin{aligned} \psi : \Omega_0 &\longrightarrow \Omega \\ \mathbf{x} &= \psi(\mathbf{X}, t), \quad \forall \mathbf{X} \in \Omega_0, \quad t \geq 0 \end{aligned}$$

The boundary of the reference configuration is denoted as  $\Gamma_0 := \partial\Omega_0$  and  $\Gamma := \partial\Omega$  represents the boundary of the current configuration. We always assume that the mapping between both boundaries is defined through the motion,  $\psi(\Gamma_0) = \Gamma$ . We denote as  $(0, T)$  the time interval of analysis.

From now on, index notation is also applied identifying a vector or tensor with its Cartesian coordinates either in the reference or the deformed configuration. As usual, repeated indexes imply summation for all space dimensions (see e.g. [1]). To denote scalars, vectors and tensor quantities we use uppercase letters when they are evaluated in the reference configuration and lowercase letters if they are reckoned in the deformed one. We employ the index zero for quantities acting in the reference configuration.

The conservation of linear momentum problem in finite strains for a total Lagrangian formulation framework consists in finding a displacement  $\mathbf{u}$  such that

$$(1) \quad \rho_0 \frac{\partial^2 u_a}{\partial t^2} - \frac{\partial}{\partial X_A} \{F_{aB} S_{BA}\} = \rho_0 b_a \quad \text{in } \Omega_0 \times (0, T)$$

where  $\rho_0$  is the initial density,  $\mathbf{F} = \frac{\partial \mathbf{x}}{\partial \mathbf{X}}$  is the deformation gradient,  $\mathbf{S}$  is the Second Piola-Kirchhoff (PK2) stress tensor and  $\mathbf{b}$  the body forces. Mass conservation implies that

$$(2) \quad \rho J = \rho_0$$

where  $J = \det \mathbf{F}$  is the Jacobian. Let us remark that due to the fact that we are solving the problem in the reference configuration only the initial density is needed. Therefore, there is no need to compute the density at every deformed configuration. With regards to the balance of angular momentum, it implies that the PK2 stress tensor must be symmetric.

In order to be capable of reproducing nearly and fully incompressible scenarios, we introduce the standard decomposition of the Cauchy stress tensor  $\boldsymbol{\sigma}$  into its volumetric and deviatoric components:

$$(3) \quad \boldsymbol{\sigma} = \boldsymbol{\sigma}' - p\mathbf{I}$$

where  $p$  is the pressure (minus the mean stress) and  $\mathbf{I}$  the identity matrix. We can now use the relation between stresses to obtain a proper decomposition for the PK2 stress tensor

[30]:

$$(4) \quad S_{AB} = JF_{Aa}^{-1}F_{Bb}^{-1}\sigma_{ab} \stackrel{(3)}{=} JF_{Aa}^{-1}F_{Bb}^{-1}\sigma'_{ab} - pJC_{AB}^{-1} := S'_{AB} - pJC_{AB}^{-1}$$

where we have introduced the deviatoric stresses  $\mathbf{S}'$  and the inverse Right Cauchy Tensor  $\mathbf{C}^{-1} = \mathbf{F}^{-1}\mathbf{F}^{-T}$ . We can now reformulate the conservation of linear momentum (1) by introducing decomposition (4):

$$(5) \quad \rho_0 \frac{\partial^2 u_a}{\partial t^2} - \frac{\partial}{\partial X_A} \{F_{aB}S'_{BA}\} + \frac{\partial}{\partial X_A} \{pJF_{Aa}^{-1}\} = \rho_0 b_a \quad \text{in } \Omega_0 \times (0, T)$$

Equation (5) allows us to formulate the linear momentum equation in terms of both displacements  $\mathbf{u}$  and pressure  $p$ . However, we will need to add an extra equation to obtain a well-posed problem. This equation will be in charge of both providing a constitutive equation for the pressure and imposing the incompressibility constraint. This constitutive equation depends on the type of material considered, and it is presented in the following section.

**2.2. Hyperelasticity.** In this work we consider isotropic hyperelastic models (See [1, 3, 30]). These models postulate the existence of a Helmholtz free-energy function (or strain energy function)  $\Psi(\mathbf{C})$  such that

$$(6) \quad \mathbf{S} = 2 \frac{\partial \Psi(\mathbf{C})}{\partial \mathbf{C}}$$

where  $\mathbf{C} = \mathbf{F}^T \mathbf{F}$  is the right Cauchy-Green tensor.

We want to deal with compressible models that can reach the incompressible limit case. To characterise such models, it is convenient to adopt a decoupled representation of the strain energy function of the specific form [1, 30]:

$$(7) \quad \Psi(\mathbf{C}) = W(\bar{\mathbf{C}}) + U(J)$$

where  $\bar{\mathbf{C}} = J^{-2/3}\mathbf{C}$  is the volume-preserving part of  $\mathbf{C}$ . Let us remark that this decomposition allows one to split the elastic response of the material into the so-called deviatoric and volumetric response, respectively. We can now write the PK2 stress tensor by introducing equation (7) into equation (6):

$$(8) \quad \mathbf{S} = 2 \frac{\partial \Psi}{\partial \mathbf{C}} = 2 \frac{\partial W}{\partial \bar{\mathbf{C}}} + 2 \frac{\partial U}{\partial J} = 2 \frac{\partial W}{\partial \bar{\mathbf{C}}} + \frac{dU}{dJ} J \mathbf{C}^{-1}$$

By comparing this equation with equation (4) we obtain that:

$$(9) \quad \mathbf{S}' = 2 \frac{\partial W}{\partial \bar{\mathbf{C}}} \quad \text{and} \quad p = -\frac{dU}{dJ}$$

Once we are able to deal with the decoupled form of the strain energy function, we describe a number of constitutive models for both the deviatoric and the volumetric components.

**2.2.1. Deviatoric models of the strain energy function.** First of all, let us recall that as we are considering isotropic hyperelastic models, the strain energy density must be written in terms of the strain invariants which are defined for the volume-preserving  $\bar{\mathbf{C}}$  by

$$(10) \quad \bar{I}_1 = \text{trace } \bar{\mathbf{C}}$$

$$(11) \quad \bar{I}_2 = \frac{1}{2} \left[ (\text{trace } \bar{\mathbf{C}})^2 - \text{trace } (\bar{\mathbf{C}}^2) \right]$$

$$(12) \quad \bar{I}_3 = \det \bar{\mathbf{C}} = \det \left( J^{-2/3} \mathbf{C} \right) = 1$$

From the strains invariants, it can be concluded that  $W(\bar{\mathbf{C}})$  must be written in terms of the first and second invariants. Let us present suitable functions for the deviatoric component of the strain energy function:

- Neo-Hookean model

This model results from considering only the first principal invariant

$$(13) \quad W(\bar{I}_1) = \frac{\mu}{2} (\bar{I}_1 - 3)$$

where  $\mu$  is the shear modulus. This function involves a single parameter and provides the simplest mathematical model for the nonlinear deformation behaviour of rubber-like materials. However, experimental data of several isotropic elastic materials cannot be reproduced by this model and it is worthwhile considering the dependency on  $\bar{I}_2$ .

- Mooney-Rivlin model

This model is derived considering the dependance on the second invariant as

$$(14) \quad W(\bar{I}_1, \bar{I}_2) = \alpha_1 (\bar{I}_1 - 3) + \alpha_2 (\bar{I}_2 - 3)$$

where  $\alpha_1$  and  $\alpha_2$  are material parameters that must satisfy  $\mu = 2(\alpha_1 + \alpha_2) > 0$ . This function is often employed in the description of the behaviour of isotropic rubber-like materials. Note that when  $\alpha_2 = 0$  we recover the Neo-Hookean model.

- Yeoh model

This model makes the assumption that the variation of the strain energy function with respect to the second invariant is equal to zero and it proposes a three-term function in terms of the first invariant

$$(15) \quad W(\bar{I}_1) = \alpha_1 (\bar{I}_1 - 3) + \alpha_2 (\bar{I}_1 - 3)^2 + \alpha_3 (\bar{I}_1 - 3)^3$$

where  $\alpha_1$ ,  $\alpha_2$  and  $\alpha_3$  are material parameters which must satisfy that  $\mu = 2\alpha_1 + 4\alpha_2 (\bar{I}_1 - 3) + 6\alpha_3 (\bar{I}_1 - 3)^2 > 0$ . This model was motivated to simulate the mechanical behaviour of carbon-black filled rubber vulcanizates.

Readers are referred to [3, 27] for further details on this kind of models.

**2.2.2. Volumetric models of the strain energy function.** Several nonlinear materials such as rubbers, polymers or soft tissues among others are often slightly compressible and associated with minor dilatational deformations. Due to the decoupled form of the strain energy density, compressibility is accounted for by the volumetric strain energy function. Let us now show some variety of models which are widely used in nonlinear computations and which depend upon the bulk modulus  $\kappa$ .

- Quadratic [31]

This model is given by the following relation:

$$(16) \quad U(J) = \frac{\kappa}{2} (J - 1)^2; \quad \frac{dU}{dJ} = \kappa (J - 1)$$

Despite of being widely used in practice, this model does not satisfy the fundamental condition of requiring an infinite amount of strain energy in order to compress the body to a single point with vanishing volume state.

- Simo et al [32]

This model circumvents previous problems by adding the logarithm of  $J$  as a principal function:

$$(17) \quad U(J) = \frac{\kappa}{4} (\log J)^2; \quad \frac{dU}{dJ} = \frac{\kappa}{2J} \log J$$

- Simo-Taylor [32]

This model satisfies all stability requirements:

$$(18) \quad U(J) = \frac{\kappa}{4} (J^2 - 1 - 2\log J); \quad \frac{dU}{dJ} = \frac{\kappa}{2} \left( J - \frac{1}{J} \right)$$

- Miehe et al [33]

In this model,  $U(J)$  is given by:

$$(19) \quad U(J) = \kappa (J - \log J - 1); \quad \frac{dU}{dJ} = \kappa \left(1 - \frac{1}{J}\right)$$

- Liu et al [34]

In this model,  $U(J)$  is expressed as:

$$(20) \quad U(J) = \kappa (J \log J - J + 1); \quad \frac{dU}{dJ} = \kappa \log J$$

- Ogden [1]

For rubber-like materials, Ogden proposed a volumetric response function in terms of the volume ratio  $J$  of the following form

$$(21) \quad U(J) = \kappa \frac{1}{\beta^2} \left( \beta \log J + J^{-\beta} - 1 \right); \quad \frac{dU}{dJ} = \frac{\kappa}{\beta J} \left(1 - \frac{1}{J^\beta}\right)$$

where  $\beta > 0$  is an empirical coefficient which must be fixed according to experimental data.

**Remark 2.1.** *It is important to note that all volumetric functions here presented can be written as  $U(J) = \kappa G(J)$ . Therefore, equation (9) can be used to obtain a proper way to impose the incompressibility of an hyperelastic material:*

$$(22) \quad p = -\frac{dU}{dJ} \quad \Leftrightarrow \quad p = -\kappa \frac{dG}{dJ} \quad \Leftrightarrow \quad \frac{p}{\kappa} + \frac{dG}{dJ} = 0$$

*This equation can be applied regardless of the compressibility of the material under study. It is interesting to observe that in the incompressible limit, when Poisson's ratio  $\nu \rightarrow 0.5$  (for isotropic materials) then  $\kappa \rightarrow \infty$  and equation (22) reduces automatically to*

$$(23) \quad \frac{dG}{dJ} = 0$$

*For all the volumetric strain energy functions presented here, equation (23) imposes directly that  $J = 1$  which is in fact the condition that a material must satisfy to be incompressible in finite strains.*

**2.3. Governing Equations.** To complete this section, we introduce the mixed solid dynamics problem which consists in finding both a displacement  $\mathbf{u}$  and a pressure  $p$  such that:

$$(24) \quad \rho_0 \frac{\partial^2 u_a}{\partial t^2} - \frac{\partial}{\partial X_A} \{F_{aB} S'_{BA}\} + \frac{\partial}{\partial X_A} \{p J F_{Aa}^{-1}\} = \rho_0 b_a \quad \text{in } \Omega_0 \times (0, T)$$

$$(25) \quad \frac{p}{\kappa} + \frac{dG}{dJ} = 0 \quad \text{in } \Omega_0 \times (0, T)$$

The governing equations must be supplied with initial conditions of the form  $\mathbf{u} = \mathbf{u}^0$ ,  $\frac{\partial \mathbf{u}}{\partial t} = \mathbf{v}^0$  in  $\Omega_0$  at  $t = 0$ , with  $\mathbf{u}^0$  and  $\mathbf{v}^0$  given, and a set of boundary conditions which can be split into Dirichlet boundary conditions (26), where the displacement is prescribed, or Neumann boundary conditions (27), where the value of tractions  $\mathbf{t}_0$  are prescribed:

$$(26) \quad \mathbf{u} = \mathbf{u}_D \quad \text{in } \Gamma_{0,D}$$

$$(27) \quad \mathbf{n}_0 \{\mathbf{FS}\} \stackrel{(4)}{=} \mathbf{n}_0 \{\mathbf{FS}'\} - p J \mathbf{n}_0 \mathbf{F}^{-T} = \mathbf{t}_0 \quad \text{in } \Gamma_{0,N}$$

where  $\mathbf{n}_0$  is the geometric unit outward normal vector on the boundary of the reference configuration  $\Gamma_0$ .

**Remark 2.2.** *Verifying that this formulation reduces to the mixed formulation in linear elasticity when infinitesimal strains theory is considered is crucial. Regarding to the momentum equation (24), the following simplifications are obtained:*

$$(28) \quad F_{aB}S'_{BA} \stackrel{(4)}{\approx} J\sigma'_{ab} \approx \left(1 + \frac{\partial u_c}{\partial x_c}\right) \sigma'_{ab} = \sigma'_{ab} + \cancel{(\nabla \cdot \mathbf{u})\sigma'_{ab}} \approx \sigma'_{ab}$$

$$(29) \quad pJ\mathbf{F}^{-1} \approx p(1 + \nabla \cdot \mathbf{u})\mathbf{I} = p\mathbf{I} + \cancel{p\nabla \cdot \mathbf{u}\mathbf{I}} \approx p\mathbf{I}$$

and taking into account that both the reference and current configurations match, we obtain the simplified momentum equation for linear elasticity

$$(30) \quad \rho \frac{\partial^2 u_a}{\partial t^2} - \frac{\partial \sigma'_{ab}}{\partial x_a} + \frac{\partial p}{\partial x_a} = \rho b_a \quad \text{in } \Omega_0 \times (0, T)$$

With respect to the incompressibility equation (25), as it was previously mentioned,  $\frac{dG}{dJ}$  is a function which imposes  $J = 1$ . Therefore,

$$(31) \quad \frac{p}{\kappa} + \frac{dG}{dJ} \approx \frac{p}{\kappa} + J - 1 \approx \frac{p}{\kappa} + (1 + \nabla \cdot \mathbf{u}) - 1 = \frac{p}{\kappa} + \nabla \cdot \mathbf{u} = 0$$

which is exactly the constitutive law of the pressure when considering linear elasticity. Let us recall that in the incompressible limit  $\kappa \rightarrow \infty$ , and this equation will reduce automatically to

$$(32) \quad \nabla \cdot \mathbf{u} = 0$$

which is the incompressibility condition for infinitesimal strain theory.

**2.4. Variational Form of the problem.** We shall use the symbol  $\langle \cdot, \cdot \rangle_\omega$  to refer the integral of the product of two functions, assuming it well-defined. This notation is simplified in the following case:  $\langle \cdot, \cdot \rangle_{\Omega_0} \equiv \langle \cdot, \cdot \rangle$ .

Let  $\mathbb{V}^d$  and  $\mathbb{Q}$  be, respectively, the proper functional spaces where displacement and pressure solutions are well-defined for each fixed time  $t \in (0, T)$ . We denote by  $\mathbb{V}_0^d$  functions in  $\mathbb{V}^d$  which vanish in the Dirichlet boundary  $\Gamma_{0,D}$ . We shall be interested also in the spaces  $\mathbb{W} := \mathbb{V} \times \mathbb{Q}$ ,  $\mathbb{W}_0 := \mathbb{V}_0 \times \mathbb{Q}$ . The variational statement of the problem is derived by testing the system (24)-(25) against arbitrary test functions,  $\mathbf{v} \in \mathbb{V}_0^d$  and  $q \in \mathbb{Q}$ . The weak form of the problem reads: find  $\mathbf{U} \equiv [\mathbf{u}, p]^T : (0, T) \rightarrow \mathbb{W}$  such that initial conditions are satisfied and

$$(33) \quad \langle \mathbf{V}, \mathfrak{D}_t(\mathbf{U}) \rangle + \mathcal{A}(\mathbf{U}, \mathbf{V}) = \mathcal{F}(\mathbf{V}) \quad \forall \mathbf{V} \in \mathbb{W}_0$$

where  $\mathcal{A}(\mathbf{U}, \mathbf{V})$  is a semilinear form defined on  $\mathbb{W} \times \mathbb{W}_0$  as

$$(34) \quad \mathcal{A}(\mathbf{U}, \mathbf{V}) := \left\langle \frac{\partial v_a}{\partial X_A}, F_{aB}S'_{BA} \right\rangle - \left\langle \frac{\partial v_a}{\partial X_A}, pJF_{Aa}^{-1} \right\rangle + \left\langle q, \frac{dG}{dJ} \right\rangle + \left\langle q, \frac{p}{\kappa} \right\rangle$$

$\mathcal{F}(\mathbf{V})$  is a linear form defined on  $\mathbb{W}_0$  as

$$(35) \quad \mathcal{F}(\mathbf{V}) := \langle v_a, \rho_0 b_a \rangle + \langle v_a, t_a \rangle_{\Gamma_{0,N}}$$

and

$$(36) \quad \mathfrak{D}_t(\mathbf{U}) := \left[ \rho_0 \frac{\partial^2 \mathbf{u}}{\partial t^2}, 0 \right]^T$$

As usual, integration by parts has been used in order to decrease the continuity requirements of unknowns  $\mathbf{u}$  and  $p$  and the traction vector  $\mathbf{t}_0$  has been identified as  $\mathbf{t}_0 = \mathbf{n}_0 \{ \mathbf{F}\mathbf{S} \} \stackrel{(4)}{=} \mathbf{n}_0 \{ \mathbf{F}\mathbf{S}' \} - pJ\mathbf{n}_0\mathbf{F}^{-T}$ .

Let us also remark that the problem can be symmetrized by multiplying (22) by an adequate function that depends on  $G$ . In that case the semilinear form  $\mathcal{A}(\mathbf{U}, \mathbf{V})$  would derive from a potential.

**2.5. Time Discretization.** In this work implicit time integrators are considered. When the material under study is either nearly or fully incompressible, the Courant-Friedrichs-Lewy (CFL) condition, which involves the bulk modulus, becomes very restrictive. If explicit time integrators are considered, extremely small time steps are needed in order to satisfy it. Furthermore, in the fully incompressible case, as  $\kappa \rightarrow \infty$ , solving the problem with explicit time integration is not possible.

Although in principle any implicit time discretization method can be applied, it has to be taken into account that an hyperbolic system of equations is being solved. It is important to control spurious high-frequency oscillations that might appear in the solution for both nearly and fully incompressible hyperelastic materials. As a consequence, numerical time integrators with high-frequency dissipation will be applied.

Let us now consider a partition of the time interval  $[0, T]$  into  $N$  time steps of size  $\delta t$ , assumed to be constant.

**2.5.1. Backward differentiation formula (BDF).** Given a generic time dependent function at a time step  $t^{n+1} = t^n + \delta t$ , for  $n = 0, 1, 2, \dots$  the approximation of the time derivative of order  $k = 1, 2, \dots$  is written using information from already computed time instants. In our problem, we have to approximate the second time derivative of the displacement,  $\frac{\partial^2 \mathbf{u}^{n+1}}{\partial t^2} := \mathbf{a}^{n+1}$ . Depending on the accuracy of the method, we can select specific formulas:

$$(37) \quad \text{BDF} : \quad \mathbf{a}^{n+1} = \frac{1}{\delta t^2} \{ \mathbf{u}^{n+1} - 2\mathbf{u}^n + \mathbf{u}^{n-1} \} + \mathcal{O}(\delta t)$$

$$(38) \quad \text{BDF2} : \quad \mathbf{a}^{n+1} = \frac{1}{\delta t^2} \{ 2\mathbf{u}^{n+1} - 5\mathbf{u}^n + 4\mathbf{u}^{n-1} - \mathbf{u}^{n-2} \} + \mathcal{O}(\delta t^2)$$

**2.5.2. Newmark- $\beta$  equations.** This is a popular class of time integrators [3]. In this time integration formula, the updated acceleration  $\mathbf{a}^{n+1}$  and velocity  $\mathbf{v}^{n+1}$  are given by:

$$(39) \quad \begin{aligned} \mathbf{a}^{n+1} &\approx \frac{1}{\beta \delta t^2} \{ \mathbf{u}^{n+1} - \mathbf{u}^n - \delta t \mathbf{v}^n - \frac{\delta t^2}{2} (1 - 2\beta) \mathbf{a}^n \} \\ \mathbf{v}^{n+1} &\approx \mathbf{v}^n + (1 - \gamma) \delta t \mathbf{a}^n + \gamma \delta t \mathbf{a}^{n+1} \end{aligned}$$

Here  $\beta$  and  $\gamma$  are parameters to be tuned. When  $\beta = \frac{1}{4}$  and  $\gamma = \frac{1}{2}$  the Newmark- $\beta$  method is implicit, unconditionally stable and at least second-order accurate.

**2.6. Linearization.** In order to solve the problem, the system needs to be linearized so that a bilinear operator which allows to compute a correction  $\delta \mathbf{U}$  of a given guess for the solution at time  $t^{n+1}$  is obtained, that we denote by  $\mathbf{U}^{n+1}$ . Iteration counters will be omitted to simplify the notation. After using a Newton-Raphson scheme, we obtain the following linearized form of the problem. Given  $\mathbf{U}^{n+1}$  as the solution at time  $t^{n+1}$  and the previous iteration, find a correction  $\delta \mathbf{U} \equiv [\delta \mathbf{u}, \delta p]^T : (0, T) \rightarrow \mathbb{W}_0$  such that

$$(40) \quad \langle \mathbf{V}, \mathfrak{D}_t(\mathbf{U}^{n+1} + \delta \mathbf{U}) \rangle + \mathcal{B}(\delta \mathbf{U}, \mathbf{V}) = \mathcal{F}(\mathbf{V}) - \mathcal{A}(\mathbf{U}^{n+1}, \mathbf{V}) \quad \forall \mathbf{V} \in \mathbb{W}_0$$

where  $\mathcal{B}(\delta \mathbf{U}, \mathbf{V})$  is the bilinear form obtained through the Newton-Raphson linearization and it is defined on  $\mathbb{W}_0 \times \mathbb{W}_0$  as

$$(41) \quad \begin{aligned} \mathcal{B}(\delta \mathbf{U}, \mathbf{V}) &= \left\langle \frac{\partial v_a}{\partial X_A}, \frac{\partial \delta u_a}{\partial X_B} S'_{BA} \right\rangle + \left\langle \frac{\partial v_a}{\partial X_A}, F_{aB} \delta S'_{BA} \right\rangle - \left\langle \frac{\partial v_a}{\partial X_A}, J p F_{Bb}^{-1} \frac{\partial \delta u_b}{\partial X_B} F_{Aa}^{-1} \right\rangle \\ &+ \left\langle \frac{\partial v_a}{\partial X_A}, J p F_{Ab}^{-1} \frac{\partial \delta u_b}{\partial X_B} F_{Ba}^{-1} \right\rangle - \left\langle \frac{\partial v_a}{\partial X_A}, J \delta p F_{Aa}^{-1} \right\rangle + \left\langle q, f(J) F_{Aa}^{-1} \frac{\partial \delta u_a}{\partial X_A} \right\rangle + \left\langle q, \frac{\delta p}{\kappa} \right\rangle \end{aligned}$$

where  $f(J)$  is a function coming from the linearization of  $\frac{dG}{dJ}$  and depends upon the volumetric strain energy function into consideration and  $\delta S'_{BA}$  is the first term in the decomposition of the PK2 tensor computed with  $\delta \mathbf{u}$ . Let us remark that all terms are evaluated at  $\mathbf{U}^{n+1}$ .

It is quite simple to observe that for every implicit time integrator presented here, we can write:

$$(42) \quad \frac{\partial^2 (\mathbf{u}^{n+1} + \delta \mathbf{u})}{\partial t^2} = \frac{C_a}{\delta t^2} \delta \mathbf{u} + \mathbf{a}^{n+1}$$

where  $C_a$  is a coefficient depending on the scheme and  $\mathbf{a}^{n+1}$  is the acceleration computed for a given iteration.

Therefore, we can write the time discretized form of  $\mathfrak{D}_t (\mathbf{U}^{n+1} + \delta \mathbf{U})$  at time step  $t^{n+1} = t^n + \delta t$  as :

$$(43) \quad \mathfrak{D}_t (\mathbf{U}^{n+1} + \delta \mathbf{U}) \approx \mathfrak{D}_{\delta u} (\delta \mathbf{U}) + \mathfrak{D}_t (\mathbf{U}^{n+1}) = \rho_0 \left[ \frac{C_a}{\delta t^2} \delta \mathbf{u}, 0 \right]^T + \rho_0 [\mathbf{a}^{n+1}, 0]^T$$

and problem (40) can be written after time discretization as:

$$(44) \quad \langle \mathbf{V}, \mathfrak{D}_{\delta u} (\delta \mathbf{U}) \rangle + \mathcal{B} (\delta \mathbf{U}, \mathbf{V}) = \mathcal{F} (\mathbf{V}) - \mathcal{A} (\mathbf{U}^{n+1}, \mathbf{V}) - \langle \mathbf{V}, \mathfrak{D}_t (\mathbf{U}^{n+1}) \rangle \quad \forall \mathbf{V} \in \mathbb{W}_0$$

**2.7. Galerkin Spatial Discretization.** The standard Galerkin approximation of this abstract variational problem is now straightforward. Let  $\mathcal{P}_h$  denote a finite element partition of the domain  $\Omega_0$ . The diameter of an element domain  $K \in \mathcal{P}_h$  is denoted by  $h_K$  and the diameter on the finite element partition by  $h = \max\{h_K | K \in \mathcal{P}_h\}$ . We can now construct conforming finite element spaces  $\mathbb{V}_h \subset \mathbb{V}$ ,  $\mathbb{Q}_h \subset \mathbb{Q}$  and  $\mathbb{W}_h = \mathbb{V}_h \times \mathbb{Q}_h$  in the usual manner, as well as the corresponding subspaces  $\mathbb{V}_{h,0} \subset \mathbb{V}_0$  and  $\mathbb{W}_{h,0} = \mathbb{V}_{h,0} \times \mathbb{Q}_h$ ,  $\mathbb{V}_{h,0}$  being made with functions that vanish on the Dirichlet boundary. In principle, functions in  $\mathbb{V}_h$  are continuous, whereas functions in  $\mathbb{Q}_h$  not necessarily.

The Galerkin discrete version of problem (44) is: For a given time  $t^{n+1}$  and a fixed iteration, find  $\delta \mathbf{U}_h \in \mathbb{W}_{h,0}$  such that

$$(45) \quad \langle \mathbf{V}_h, \mathfrak{D}_{\delta u} (\delta \mathbf{U}_h) \rangle + \mathcal{B} (\delta \mathbf{U}_h, \mathbf{V}_h) = \mathcal{F} (\mathbf{V}_h) - \mathcal{A} (\mathbf{U}_h^{n+1}, \mathbf{V}_h) - \langle \mathbf{V}_h, \mathfrak{D}_t (\mathbf{U}_h^{n+1}) \rangle \quad \forall \mathbf{V}_h \in \mathbb{W}_{h,0}$$

The well posedness of this problem relies on an inf-sup condition [5]. This condition is necessary and sufficient for the existence and uniqueness of the solution to the discrete saddle-point problem. Convenient displacement-pressure interpolations, such as equal interpolation, turn out to violate the inf-sup condition. This is why the so-called stabilized formulations have been proposed to approximate this kind of problems. The main idea is to replace (44) by another discrete variational problem in which the bilinear form  $\mathcal{B}$  is enhanced so that it has improved stability properties. In order to overcome the instabilities previously discussed, we propose the stabilization technique described in the next section.

**Remark 2.3.** *Taking a look on the bilinear form  $\mathcal{B}$  one should notice that the only term which involves  $q$  and  $\delta p$  is  $\frac{1}{\kappa} \langle q, \delta p \rangle$ . Hence, in the nearly and fully incompressible cases, when  $\kappa \rightarrow \infty$ , this term vanishes causing the saddle-point structure of the problem to appear.*

### 3. INCOMPRESSIBLE SOLID DYNAMICS STABILIZED FINITE ELEMENT FORMULATION

The stabilized finite element method we propose in the following is based on the VMS concept [15, 35]. Let  $\mathbb{W} = \mathbb{W}_h \oplus \tilde{\mathbb{W}}$ , where  $\tilde{\mathbb{W}}$  is any space to complete  $\mathbb{W}_h$  in  $\mathbb{W}$ .  $\tilde{\mathbb{W}}$  will be approximated by a finite-dimensional space despite the fact that it is infinite-dimensional. The elements of this space are denoted by  $\tilde{\mathbf{U}} \equiv [\tilde{\mathbf{u}}, \tilde{p}]^T$  and they are called subscales. Likewise, let  $\mathbb{W}_0 = \mathbb{W}_{h,0} \oplus \tilde{\mathbb{W}}_0$ .

Taking into account that  $\mathcal{B}$  is a bilinear form, the continuous problem (44) is equivalent to find  $\delta\mathbf{U} \in \mathbb{W}_h$  and  $\tilde{\mathbf{U}} \in \tilde{\mathbb{W}}$  such that

$$(46) \quad \begin{aligned} & \langle \mathbf{V}_h, \mathfrak{D}_{\delta u}(\delta\mathbf{U}_h) \rangle + \langle \mathbf{V}_h, \mathfrak{D}_{\delta u}(\tilde{\mathbf{U}}) \rangle + \mathcal{B}(\delta\mathbf{U}_h, \mathbf{V}_h) + \mathcal{B}(\tilde{\mathbf{U}}, \mathbf{V}_h) \\ & = \mathcal{F}(\mathbf{V}_h) - \mathcal{A}(\mathbf{U}_h^{n+1}, \mathbf{V}_h) - \langle \mathbf{V}_h, \mathfrak{D}_t(\mathbf{U}_h^{n+1}) \rangle \quad \forall \mathbf{V}_h \in \mathbb{W}_{h,0} \end{aligned}$$

$$(47) \quad \begin{aligned} & \langle \tilde{\mathbf{V}}, \mathfrak{D}_{\delta u}(\delta\mathbf{U}_h) \rangle + \langle \tilde{\mathbf{V}}, \mathfrak{D}_{\delta u}(\tilde{\mathbf{U}}) \rangle + \mathcal{B}(\delta\mathbf{U}_h, \tilde{\mathbf{V}}) + \mathcal{B}(\tilde{\mathbf{U}}, \tilde{\mathbf{V}}) \\ & = \mathcal{F}(\tilde{\mathbf{V}}) - \mathcal{A}(\mathbf{U}_h^{n+1}, \tilde{\mathbf{V}}) - \langle \tilde{\mathbf{V}}, \mathfrak{D}_t(\mathbf{U}_h^{n+1}) \rangle \quad \forall \tilde{\mathbf{V}} \in \tilde{\mathbb{W}} \end{aligned}$$

where equation (46) is called finite element scale equation and (47) is called the subgrid scale equation.

The main idea behind any stabilized finite element method derived from the VMS framework is to obtain an expression for the subscales from the subgrid scale equation (47) in order to complement our finite element scale equation (46). First of all let us make some assumptions about the subgrid scale functions. In this work we consider the subscales to be quasi-static, which means that they are not time-dependent:

$$(48) \quad \frac{\partial^2 \tilde{\mathbf{u}}}{\partial t^2} \approx \mathbf{0} \quad \Leftrightarrow \quad \mathfrak{D}_{\delta u}(\tilde{\mathbf{U}}) \approx [0, 0]^T$$

**Remark 3.1.** *Note that the contribution from the transient evolution of the subscales can be kept. In this case, the subscales are called to be time-dependent or dynamic subscales [13]. The cost it implies is the storage of the subscales in previous time steps.*

We also assume the subscale to behave as bubble functions, which means that they vanish across inter-element boundaries. Taking this into account, we can integrate by parts within each element in equation (47) to obtain:

$$(49) \quad \begin{aligned} & \sum_K \langle \tilde{\mathbf{V}}, \mathfrak{D}_{\delta u}(\delta\mathbf{U}_h) \rangle_K + \sum_K \langle \tilde{\mathbf{V}}, \mathfrak{B}(\delta\mathbf{U}_h) \rangle_K + \sum_K \langle \tilde{\mathbf{V}}, \mathfrak{B}(\tilde{\mathbf{U}}) \rangle_K \\ & = \sum_K \langle \tilde{\mathbf{V}}, \mathfrak{F} \rangle_K - \sum_K \langle \tilde{\mathbf{V}}, \mathfrak{A}(\mathbf{U}_h^{n+1}) \rangle_K - \sum_K \langle \tilde{\mathbf{V}}, \mathfrak{D}_t(\mathbf{U}_h^{n+1}) \rangle_K \quad \forall \tilde{\mathbf{V}} \in \tilde{\mathbb{W}} \end{aligned}$$

where  $\sum_K$  stands for the summation over all  $K \in \mathcal{P}_h$  and  $\mathfrak{B}(\delta\mathbf{U}_h) = [\mathfrak{B}_u(\delta\mathbf{U}_h), \mathfrak{B}_p(\delta\mathbf{U}_h)]^T$  is a linear operator coming from the integration by parts of  $\mathcal{B}$  such that  $\mathcal{B}(\delta\mathbf{U}_h, \tilde{\mathbf{V}}) = \sum_K \langle \tilde{\mathbf{V}}, \mathfrak{B}(\delta\mathbf{U}_h) \rangle_K$  and it is defined as:

$$\begin{aligned} \mathfrak{B}_u(\delta\mathbf{U}_h)_a &= -\frac{\partial}{\partial X_A} \left\{ \frac{\partial \delta u_{h,a}}{\partial X_B} S'_{BA} \right\} - \frac{\partial}{\partial X_A} \left\{ F_{AB} \delta S'_{BA} \right\} + \frac{\partial}{\partial X_A} \left\{ J p_h F_{Bb}^{-1} \frac{\partial \delta u_{h,b}}{\partial X_B} F_{Aa}^{-1} \right\} \\ &\quad - \frac{\partial}{\partial X_A} \left\{ J p_h F_{Ab}^{-1} \frac{\partial \delta u_{h,b}}{\partial X_B} F_{Ba}^{-1} \right\} + \frac{\partial}{\partial X_A} \left\{ J \delta p_h F_{Aa}^{-1} \right\} \\ \mathfrak{B}_p(\delta\mathbf{U}_h) &= f(J) F_{Aa}^{-1} \frac{\partial \delta u_{h,a}}{\partial X_A} \end{aligned}$$

A similar expression is found for  $\mathfrak{B}(\tilde{\mathbf{U}})$  in (49).

Regarding to the right-hand side,  $\mathfrak{F} = [\mathfrak{F}_u, \mathfrak{F}_p]^T$  appears from the external forces form  $\mathcal{F}$  and it is given by:

$$(50) \quad \mathfrak{F}_{u,a} = \rho_0 b_a \quad ; \quad \mathfrak{F}_p = 0$$

and finally  $\mathfrak{A}(\mathbf{U}_h^{n+1}) = [\mathfrak{A}_u(\mathbf{U}_h^{n+1}), \mathfrak{A}_p(\mathbf{U}_h^{n+1})]^T$  comes from the integration by parts of  $\mathcal{A}$  and it is defined as:

$$(51) \quad \begin{aligned} \mathfrak{A}_u(\mathbf{U}_h^{n+1})_a &= -\frac{\partial}{\partial X_A} \{F_{aB} S'_{BA}\} + \frac{\partial}{\partial X_A} \{J p_h F_{Aa}^{-1}\} \\ \mathfrak{A}_p(\mathbf{U}_h^{n+1}) &= \frac{dG}{dJ} \end{aligned}$$

**Remark 3.2.** *In the case of linear elements, for which second order derivatives of finite element functions in the element interiors vanish, these expressions reduce significantly so that it is worthwhile to make them explicit:*

$$\begin{aligned} \mathfrak{B}_u(\delta \mathbf{U}_h)_a &= J \frac{\partial p_h}{\partial X_A} F_{Bb}^{-1} \frac{\partial \delta u_{h,b}}{\partial X_B} F_{Aa}^{-1} - J \frac{\partial p_h}{\partial X_A} F_{Ab}^{-1} \frac{\partial \delta u_{h,b}}{\partial X_B} F_{Ba}^{-1} + J \frac{\partial \delta p_h}{\partial X_A} F_{Aa}^{-1} \\ \mathfrak{A}_u(\mathbf{U}_h^{n+1}) &= J \frac{\partial p_h}{\partial X_A} F_{Aa}^{-1} \end{aligned}$$

Equation (49) must be satisfied for all elements  $K \in \mathcal{P}_h$  and for any  $\tilde{\mathbf{V}} \in \tilde{\mathbb{W}}$ , which strictly enforces that:

$$(52) \quad \tilde{\Pi} \left( \mathfrak{D}_{\delta u}(\delta \mathbf{U}_h) + \mathfrak{B}(\delta \mathbf{U}_h) + \mathfrak{B}(\tilde{\mathbf{U}}) \right) = \tilde{\Pi} \left( \mathfrak{F} - \mathfrak{A}(\mathbf{U}_h^{n+1}) - \mathfrak{D}_t(\mathbf{U}_h^{n+1}) \right)$$

where  $\tilde{\Pi}$  is the  $L^2$  projection onto the space of subscales. This equation allows us to obtain a way to obtain an expression for the subscales:

$$(53) \quad \tilde{\Pi} \left( \mathfrak{B}(\tilde{\mathbf{U}}) \right) = \tilde{\Pi} \left( \mathfrak{A}(\delta \mathbf{U}_h, \mathbf{U}_h^{n+1}) \right)$$

where  $\mathfrak{A}(\delta \mathbf{U}_h, \mathbf{U}_h^{n+1}) := \mathfrak{F} - \mathfrak{A}(\mathbf{U}_h^{n+1}) - \mathfrak{D}_t(\mathbf{U}_h^{n+1}) - \mathfrak{D}_{\delta u}(\delta \mathbf{U}_h) - \mathfrak{B}(\delta \mathbf{U}_h)$ .

The idea now is to approximate operator  $\mathfrak{B}$  by a matrix  $\tau_K^{-1}$  within each element  $K$ . Since we may consider that  $\tau_K^{-1} \tilde{\mathbf{U}}$  already belongs to the space of subscales,  $\tilde{\Pi}(\tau_K^{-1} \tilde{\mathbf{U}}) = \tau_K^{-1} \tilde{\mathbf{U}}$ , and from (53) we obtain:

$$(54) \quad \tilde{\mathbf{U}} \approx \tau_K \tilde{\Pi} \left( \mathfrak{A}(\delta \mathbf{U}_h, \mathbf{U}_h^{n+1}) \right) \quad \text{in } K \in \mathcal{P}_h$$

where  $\tau_K$  is a matrix of algorithmic parameters depending on  $K$  and the operator  $\mathfrak{B}$ . This approximation for  $\tilde{\mathbf{U}}$  is intended to mimic the effect of  $\mathfrak{B}(\tilde{\mathbf{U}})$  in the volume integral (46). Matrix  $\tau_K$  will be called the matrix of stabilization parameters. According to the heuristic approach proposed in [13] for the study of transient incompressible flows and its extension to material nonlinear problems in [11] we simplify the stabilization matrix by a diagonal one:

$$(55) \quad \tau_K \approx \begin{pmatrix} \tau_u \mathbf{I} & \mathbf{0} \\ \mathbf{0} & \tau_p \end{pmatrix}$$

where  $\tau_u$  and  $\tau_p$  are coefficients coming from the study of the behaviour of the stabilization parameters based on a Fourier analysis of the problem for the subscales. In this work, we propose to use the stabilization parameters proposed in [11] for linear elastic cases:

$$(56) \quad \tau_u = c_1 \frac{h_K^2}{2\mu} \quad \text{and} \quad \tau_p = 2c_2 \mu$$

where  $c_1$  and  $c_2$  are algorithmic parameters which must be determined.

Finally, equation (54) can be introduced into the finite element scale equation (46) to obtain the following problem:

$$(57) \quad \begin{aligned} \langle \mathbf{V}_h, \mathfrak{D}_{\delta u}(\delta \mathbf{U}_h) \rangle + \mathcal{B}(\delta \mathbf{U}_h, \mathbf{V}_h) + \sum_K \tau_K \left\langle \mathfrak{L}(\mathbf{V}_h), \tilde{\Pi} \left( \mathfrak{A}(\delta \mathbf{U}_h, \mathbf{U}_h^{n+1}) \right) \right\rangle \\ = \mathcal{F}(\mathbf{V}_h) - \mathcal{A}(\mathbf{U}_h^{n+1}, \mathbf{V}_h) - \langle \mathbf{V}_h, \mathfrak{D}_t(\mathbf{U}_h^{n+1}) \rangle \quad \forall \mathbf{V}_h \in \mathbb{W}_{h,0} \end{aligned}$$

where  $\mathfrak{L}(\mathbf{V}_h) = [\mathfrak{L}_u(\mathbf{V}_h), \mathfrak{L}_p(\mathbf{V}_h)]^T$  is a linear operator coming from the integration by parts of  $\mathcal{B}$  such that  $\mathcal{B}(\tilde{\mathbf{U}}, \mathbf{V}_h) = \sum_K \langle \mathfrak{L}(\mathbf{V}_h), \tilde{\mathbf{U}} \rangle_K$  and it is defined as:

$$(58) \quad \begin{aligned} \mathfrak{L}_u(\mathbf{V}_h)_a &= -\frac{\partial}{\partial X_A} \left\{ \frac{\partial \delta v_{h,a}}{\partial X_B} S'_{AB} \right\} + \frac{\partial}{\partial X_A} \left\{ J p_h F_{Aa}^{-1} \frac{\partial v_{h,b}}{\partial X_B} F_{Bb}^{-1} \right\} \\ &\quad - \frac{\partial}{\partial X_A} \left\{ J p_h F_{Ba}^{-1} \frac{\partial v_{h,b}}{\partial X_B} F_{Ab}^{-1} \right\} - \frac{\partial}{\partial X_A} \{ q f(J) F_{Aa}^{-1} \} \\ \mathfrak{L}_p(\mathbf{V}_h) &= \frac{\partial v_{h,a}}{\partial X_A} J F_{Aa}^{-1} \end{aligned}$$

There exist several stabilization methods coming from the VMS technique depending on the selection of the projection onto the subscales space. In this work, two different options are considered.

**3.1. Algebraic SubGrid Scales (ASGS).** This is the simplest choice. We take the projection onto the subscales space as the identity when applied to the residual (see [36] for further details), so that

$$(59) \quad \tilde{\Pi}(\mathfrak{R}(\delta \mathbf{U}_h, \mathbf{U}_h^{n+1})) = \mathfrak{R}(\delta \mathbf{U}_h, \mathbf{U}_h^{n+1})$$

and we obtain as a final stabilized formulation

$$(60) \quad \begin{aligned} &\langle \mathbf{V}_h, \mathfrak{D}_{\delta u}(\delta \mathbf{U}_h) \rangle + \mathcal{B}(\delta \mathbf{U}_h, \mathbf{V}_h) + \sum_K \tau_K \langle \mathfrak{L}(\mathbf{V}_h), \mathfrak{R}(\delta \mathbf{U}_h, \mathbf{U}_h^{n+1}) \rangle \\ &= \mathcal{F}(\mathbf{V}_h) - \mathcal{A}(\mathbf{U}_h^{n+1}, \mathbf{V}_h) - \langle \mathbf{V}_h, \mathfrak{D}_t(\mathbf{U}_h^{n+1}) \rangle \quad \forall \mathbf{V}_h \in \mathbb{W}_{h,0} \end{aligned}$$

**3.2. Orthogonal Subgrid Scales (OSS).** In [37] it is argued that a natural approximation for the unknown subgrid space is to take it orthogonal to the finite element space:

$$(61) \quad \tilde{\Pi}(\mathfrak{R}(\delta \mathbf{U}_h, \mathbf{U}_h^{n+1})) = \mathfrak{R}(\delta \mathbf{U}_h, \mathbf{U}_h^{n+1}) - \Pi^h(\mathfrak{R}(\mathbf{U}_h^{n+1}))$$

where  $\Pi^h$  is the  $L^2$  projection onto the finite element space. Due to the fact that this projection must increase the size of our system if we compute it in an implicit way, we have decided to approximate it with the residual of the previous time step. The final form of the stabilized problem with OSS method emerges as:

$$(62) \quad \begin{aligned} &\langle \mathbf{V}_h, \mathfrak{D}_{\delta u}(\delta \mathbf{U}_h) \rangle + \mathcal{B}(\delta \mathbf{U}_h, \mathbf{V}_h) + \sum_K \tau_K \langle \mathfrak{L}(\mathbf{V}_h), \mathfrak{R}(\delta \mathbf{U}_h, \mathbf{U}_h^{n+1}) \rangle \\ &= \mathcal{F}(\mathbf{V}_h) - \mathcal{A}(\mathbf{U}_h^{n+1}, \mathbf{V}_h) - \langle \mathbf{V}_h, \mathfrak{D}_t(\mathbf{U}_h^{n+1}) \rangle \\ &+ \sum_K \tau_K \langle \mathfrak{L}(\mathbf{V}_h), \Pi^h(\mathfrak{R}(\mathbf{U}_h^{n+1})) \rangle \quad \forall \mathbf{V}_h \in \mathbb{W}_{h,0} \end{aligned}$$

**Remark 3.3.** *A key property of the OSS stabilization is that, thanks to the projection onto the finite element space, we keep the consistency of the formulation in a weakly sense in spite of including just the minimum number of terms to stabilize the solution.*

#### 4. NUMERICAL EXAMPLES

In this section, several numerical examples are presented to assess the performance of the proposed formulation. In the first example, we evaluate the performance of our finite element formulation in the incompressible limit through the standard Cook's membrane test. The second case we consider is a bending problem for a beam-like structure in order to show the behaviour of the method in incompressible bending dominated scenarios. Finally, a twisting column is set which presents extreme nonlinear deformations. All these examples are widely used in incompressible hyperelastic cases [24, 25, 27, 28].

For all the numerical examples included next, hyperelastic models are considered fully incompressible, and so the bulk modulus is  $\kappa = \infty$ . As previously discussed, the nonlinearities in the problem are solved via a Newton-Raphson scheme. Depending on the nonlinearities, the initial guess of the iterative procedure needs to be close enough to the solution to guarantee convergence of the nonlinear iterations. In time-depending schemes, the time step is the parameter which controls the evolution of the nonlinear iterations, so we will have to tune it depending on the nonlinearities of each numerical example. A maximum of 10 iterations is set, and the numerical tolerance for the  $L^2$  norm is  $10^{-7}$ . In order to solve the monolithic system of linear equations, we use the Biconjugate Gradients solver, `BiCGstab` [38], which is already implemented in the `PETSc` parallel solver library [39].

**Remark 4.1.** *Some works prefer to choose the time step size based on either the characteristic shear wave speed or the stabilization parameter size. We prefer not to use this approach since it mixes the definition of the stabilization parameter with the time discretization of the problem.*

**4.1. Plane Strain Cook's Membrane.** In this case, we study the dynamic Cook's membrane, a bending dominated example. This is the standard test used by many authors as a reference test to check their formulations. Although this test was firstly introduced for static cases [10, 27], an extension to transient problems can be found in [28]. We are going to keep the finite strain assumption in order to evaluate our nonlinear finite element formulation, even if in this case the strains could be considered small.

The problem consists of a tapered panel, clamped on the left side and subjected to a shearing vertical load at the free right edge,  $\mathbf{t}_0 = (0, 6.25)$  Pa. Stress free boundary conditions are applied on the remaining boundaries. We set a NeoHookean material with Young Modulus  $E = 250$  Pa and density  $\rho_0 = 1$  kg/m<sup>3</sup>. To define the deviatoric part of the material, we consider a Quadratic law. The initial conditions are  $\mathbf{u}^0 = \mathbf{0}$  and  $\mathbf{v}^0 = \mathbf{0}$ . The geometry of this problem is shown in Figure 1a.

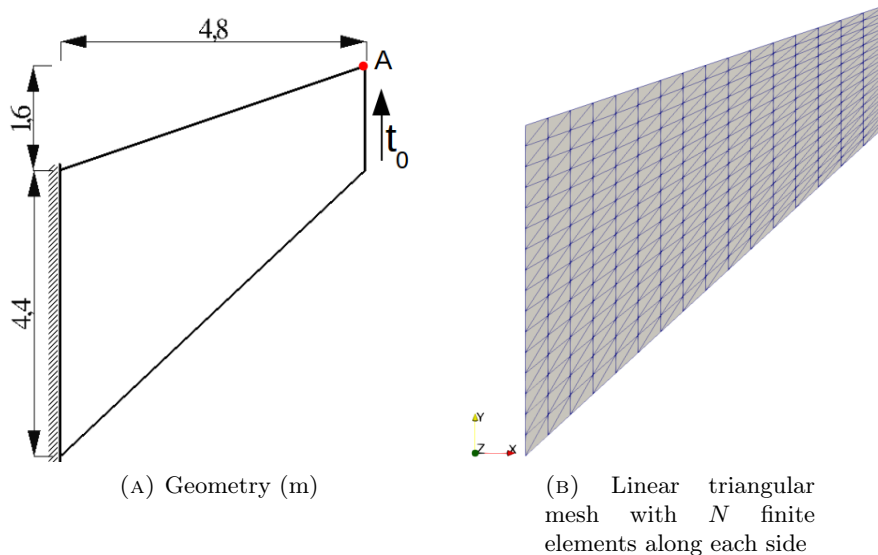


FIGURE 1. Cook's membrane problem. Geometry (1a) and an example of a linear triangular mesh (1b).

In order to test the evolution of the solution while refining our mesh, the problem has been discretized into linear triangular structured meshes with  $N$  finite elements along each side (see Figure 1b).

In Figure 2, we present a comparison of the vertical displacement at point A at  $t = 7$  s using the mixed formulation without stabilization and stabilized with both the ASGS and the OSS methods. For all cases, we fix time step as  $\delta t = 0.05$  s and the BDF2 time integration scheme is applied.

**Remark 4.2.** *In this case, we have selected BDF2 in order to ensure that the numerical dissipation introduced by the time integration scheme is enough to eliminate the nonphysical high-frequency modes appearing in the numerical solution (see Figure 4).*

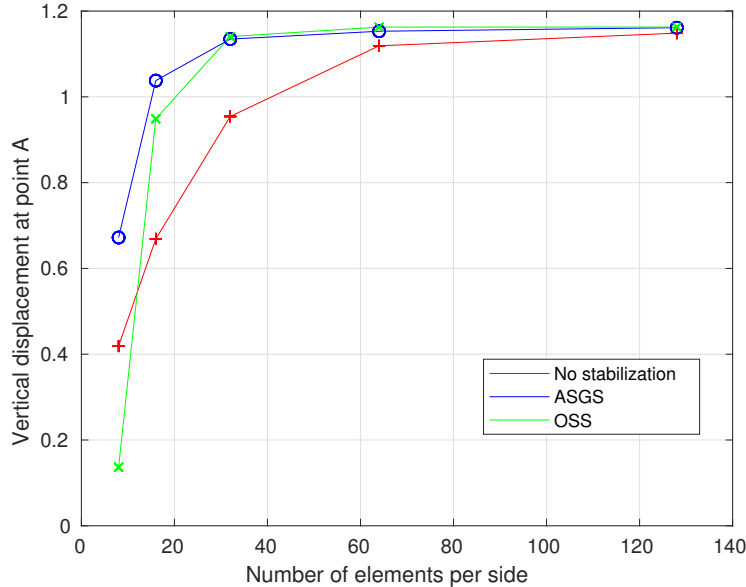


FIGURE 2. Cook’s membrane problem. Convergence of the vertical displacement (m) at point A at  $t = 7$  s.

Figure 2 illustrates the convergence of our mixed proposed formulation depending on the chosen stabilization. Both OSS and ASGS deal appropriately with the incompressibility constraint whereas when no stabilization is considered we observe a poor convergence rate. Despite the fact that the momentum equation does not need to be stabilized, the error introduced for the constitutive law of the pressure causes the poor accuracy of the displacement. As expected, the proposed stabilized mixed formulation does not exhibit volume locking for neither the ASGS nor the OSS methods.

It is interesting to observe that the ASGS stabilization method behaves better than the OSS one only for really coarse meshes. This behaviour is justified due to the fact that in the OSS technique, we are approximating the projection onto the finite element space evaluated in the previous time step. This approximation may be introducing an error that clearly depends on the mesh as well as the time step size.

For the sake of completeness, Figure 3 shows the pressure field for the three cases and the deformed solution at  $t = 7$  s. As mentioned before, when no stabilization is applied, pressure gradients appear over the inner element boundaries due to the jumps of pressure values in the elements as it can be observed in Figure 3a. On the other hand, we can see that both the ASGS and the OSS methods yield the pressure field properly, as it is shown in Figure 3b and Figure 3c. Let us remark that the OSS method is able to concentrate more accurately the maximum values of the pressure.

In order to study the relation between the different proposed formulations with the several time integration schemes we have introduced in this work, we show in Figure 4 the

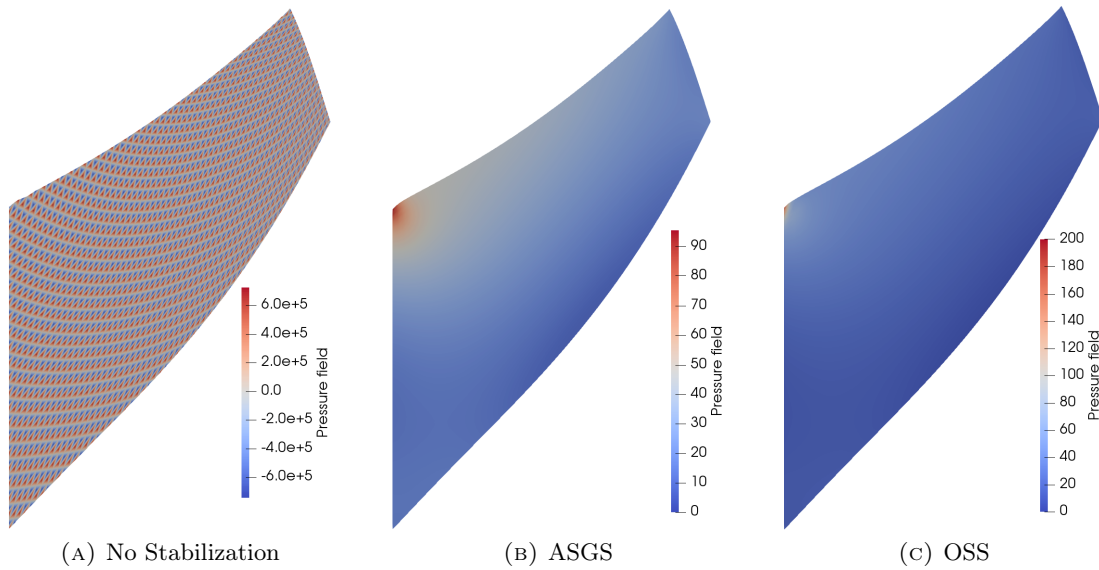


FIGURE 3. Cook's membrane problem. Pressure field (Pa) for a  $64 \times 64 \times 2$  triangular linear mesh.

evolution up to  $T = 7$  s of both the vertical displacement and the pressure at the right top corner of the membrane for  $\delta t = 0.05$  s and for a fixed  $128 \times 128 \times 2$  linear triangular mesh.

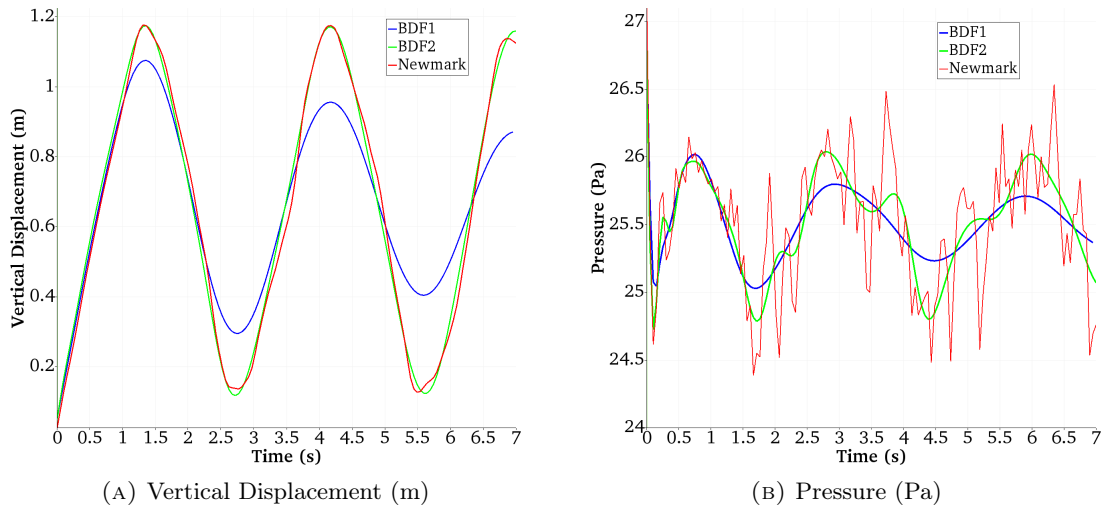


FIGURE 4. Cook's membrane problem. Comparison between several time integrators with  $\delta t = 0.05$  s and a linear triangular mesh with 128 elements per side.

The comparison of the BDF1, the BDF2 and the Newmark time integrators of Figure 4 clearly demonstrates the following facts. On the one hand, BDF1 is only first-order accurate and it is highly dissipative, affecting the accuracy of the method by eliminating physical modes of the pressure. On the other hand, in spite of the fact that Newmark scheme is second-order for  $\beta = \frac{1}{4}$  and  $\gamma = \frac{1}{2}$ , it does introduce any numerical dissipation, which would help preventing high frequency oscillations of unphysical modes. With regards

to BDF2, it is seen that it is able to dissipate the nonphysical modes while keeping the accuracy of the method and it can be safely used.

**Remark 4.3.** *In order to overcome the problem described with the Newmark scheme, several time integrators have been introduced over last decades, including the Generalized- $\alpha$  method [40], to control the numerical dissipation that needs to be added to the system.*

**4.2. A 3D bending beam problem.** As a second test in finite elasticity, we consider a three dimensional beam of square section clamped on its bottom face very similar to the one presented in [27]. The initial geometry is a parallelepiped of dimension  $1 \times 1 \times 6$  m as shown in Figure (5a). We consider stress free conditions and zero displacement initial conditions are applied.

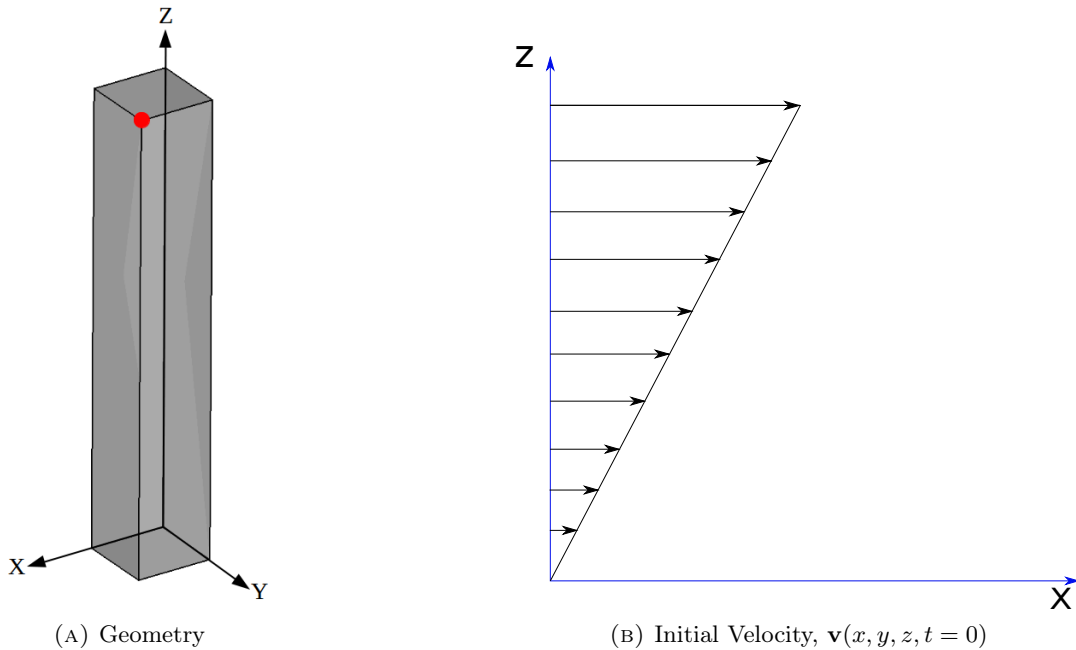


FIGURE 5. Bending beam. Geometry (5a) and Initial Velocity Field (5b).

In order to initialize the bending of the column, we impose an initial velocity condition (5b):

$$(63) \quad \mathbf{v}^0(x, y, z) = \left( \frac{5}{3}z, 0, 0 \right)^T \quad \text{m/s}$$

The initial displacement field is  $\mathbf{u}^0 = \mathbf{0}$ .

The material is considered Mooney-Rivlin with initial density  $\rho_0 = 1.1 \times 10^3$  kg/m<sup>3</sup>,  $\alpha_1 = 0.182$  MPa and  $\alpha_2 = 9.79 \times 10^{-3}$  MPa, identical to the one proposed in [28]. Due to the fact that the beam is clamped on its bottom face, we impose homogeneous boundary conditions for the displacement field. The rest of the boundary is prescribed with zero traction.

The interest of this example is to show the performance of the proposed formulation in bending dominated scenarios. As explained before, this method is independent of the kind of hyperelastic material model. Therefore, we have selected a Mooney-Rivlin model to simulate this bending dominated problem. The main goal of this example is to show that our stabilized mixed formulation works properly in bending dominated scenarios and in 3D cases for truly incompressible materials. For this reason, we have selected 3 different linear tetrahedral meshes:

Mesh	Number of elements
1	$6 \times 6 \times 36 \times 6$
2	$8 \times 8 \times 48 \times 6$
3	$12 \times 12 \times 72 \times 6$

In order to avoid unphysical modes appearing from the time integration scheme, we have selected the high-dissipative BDF2 time integrator with time step  $\delta t = 0.01$  s.

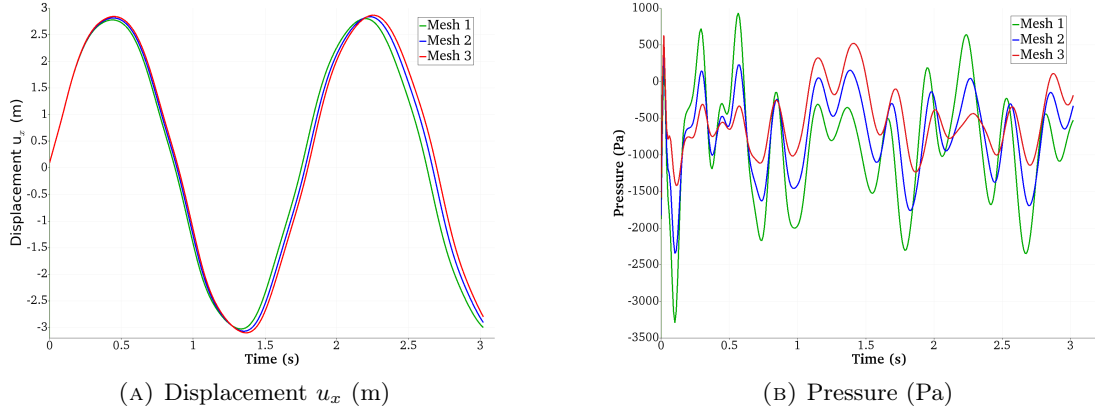


FIGURE 6. Bending beam. Comparison between several meshes with  $\delta t = 0.01$  s and ASGS as stabilization technique.

Figure 6 displays a comparison among several refinement levels up to  $T = 3$  s at the red point of Figure 5a. Figure 6 clearly shows the effectiveness of the proposed scheme to produce locking-free behaviour without spurious oscillations in the pressure field. It is interesting to see that even for very coarse meshes like Mesh 1, where the spatial error is propagated along time, the method is able to capture well-solved fields without unphysical modes in the pressure field.

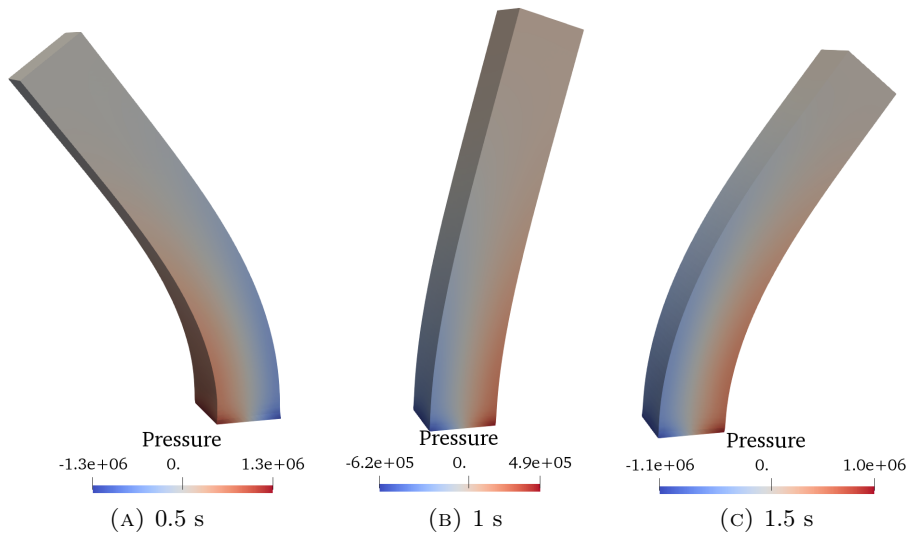


FIGURE 7. Bending beam. Deformation and pressure field (Pa) for  $\delta t = 0.01$  s with ASGS stabilization technique.

To end up this problem, Figures 7 and 8 show the evolution of the deformation and the pressure field along time up to  $T = 3$  s for Mesh 3. It can be observed that the deformation

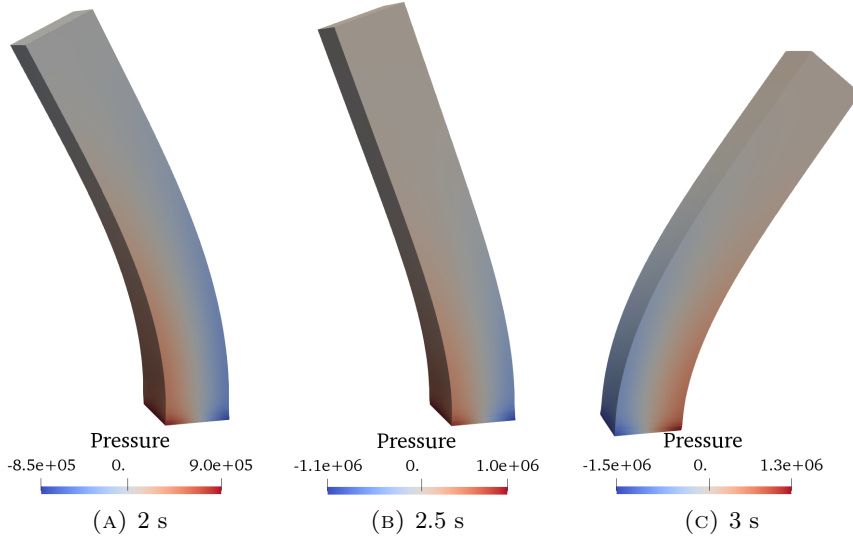


FIGURE 8. Bending beam. Deformation and pressure field for  $\delta t = 0.01$  s with ASGS stabilization technique.

is accurately reproduced even for complex hyperelastic material models like the Mooney-Rivlin model in fully incompressible scenarios. Regarding the pressure field, we can state that it is correctly captured by our mixed formulation, placing the maximum values of the pressure at the bottom of the beam, where the structure is clamped and where they are expected to appear.

**4.3. Twisting column.** As a final example, we present the twisting column test. This test is widely used to assess the robustness of any formulation in extreme nonlinear deformations [24, 25, 27, 28].

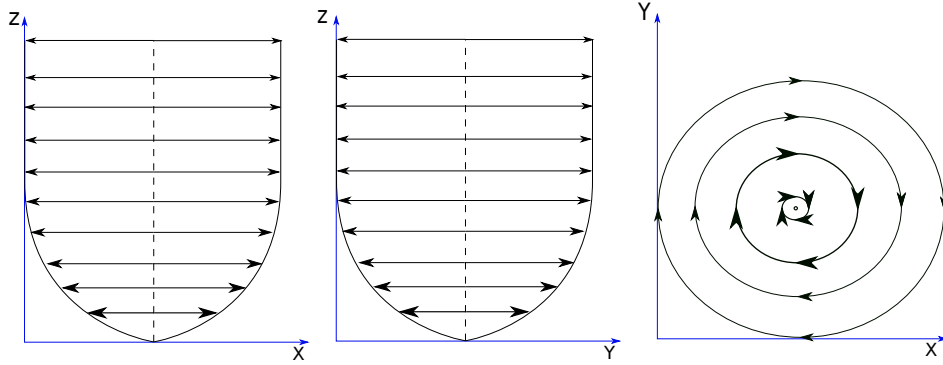


FIGURE 9. Twisting column. Initial Velocity Field.

The geometry is identical to the bending beam described in the previous example. The beam is also clamped on its bottom face. In order to make the column twist, we apply an initial sinusoidal velocity field:

$$(64) \quad \mathbf{v}^0(x, y, z) = \Omega \sin\left(\frac{\pi z}{12}\right) (y, -x, 0)^T \quad \text{m/s}$$

The material is considered Neo-Hookean with initial density  $\rho_0 = 1.1 \times 10^3$  kg/m<sup>3</sup>, Young modulus  $E = 1.7 \times 10^7$  Pa and Poisson ratio  $\nu = 0.5$ . To define the deviatoric part of the material, we consider a Simo-Taylor law. The geometry of the column is shown in Figure 5a and the applied initial velocity in Figure 9. Several levels of refinement have

been considered to perform the computations. To construct the meshes, we start with hexahedral elements which are further subdivided into 6 tetrahedral ones each. So we consider 3 different meshes. Mesh 1, with  $8 \times 8 \times 48 \times 6$  linear finite elements, Mesh 2 with  $12 \times 12 \times 72 \times 6$  elements and we end up with Mesh 3 with  $16 \times 16 \times 96 \times 6$  elements. We consider the BDF2 time integrator.

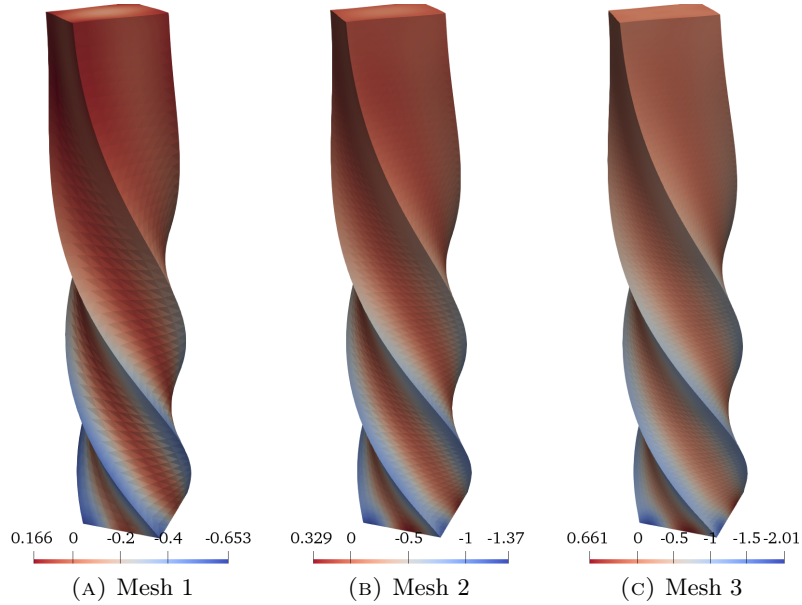


FIGURE 10. Twisting column. Deformation and pressure field (MPa) for  $\delta t = 0.01$  s at  $t = 0.1$  s with the OSS stabilization technique.

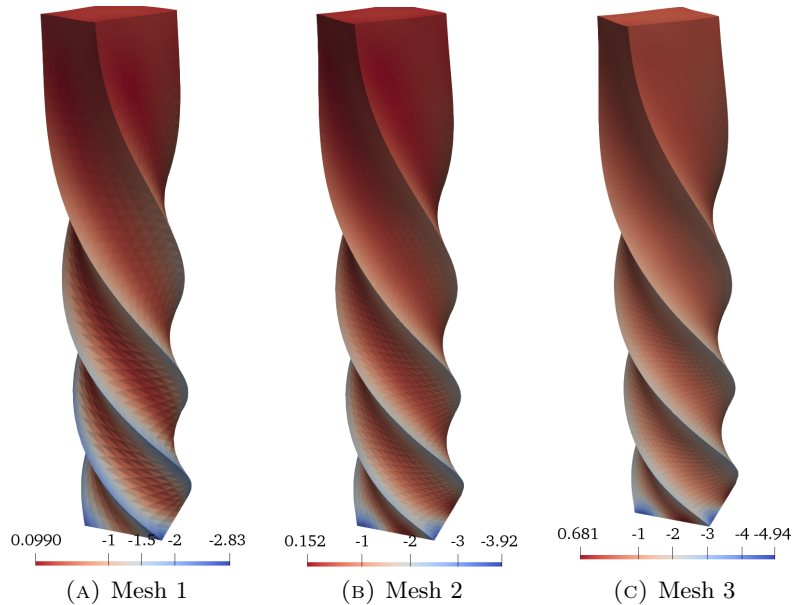


FIGURE 11. Twisting column. Deformation and pressure field (MPa) for  $\delta t = 0.001$  s at  $t = 0.1$  s with the OSS stabilization technique.

The deformation and the pressure field are shown for  $t = 0.1$  s and  $t = 0.3$  s in Figures 10, 11 and Figures 12, 13 respectively. We have included the results for  $\delta t = 0.01$  s and  $\delta t = 0.001$  s in order to observe the roll of the time step.

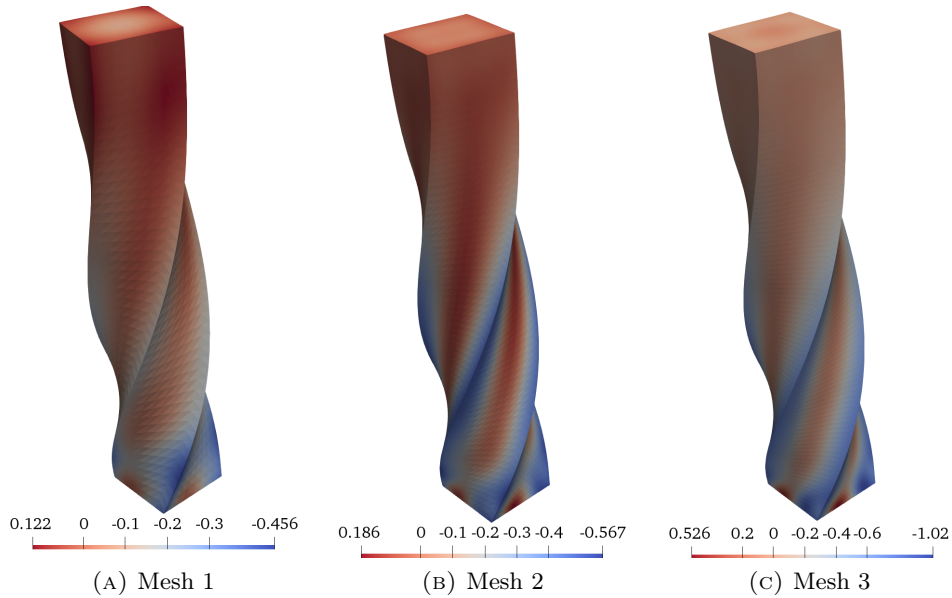


FIGURE 12. Twisting column. Deformation and pressure field (MPa) for  $\delta t = 0.01$  s at  $t = 0.3$  s with the OSS stabilization technique.

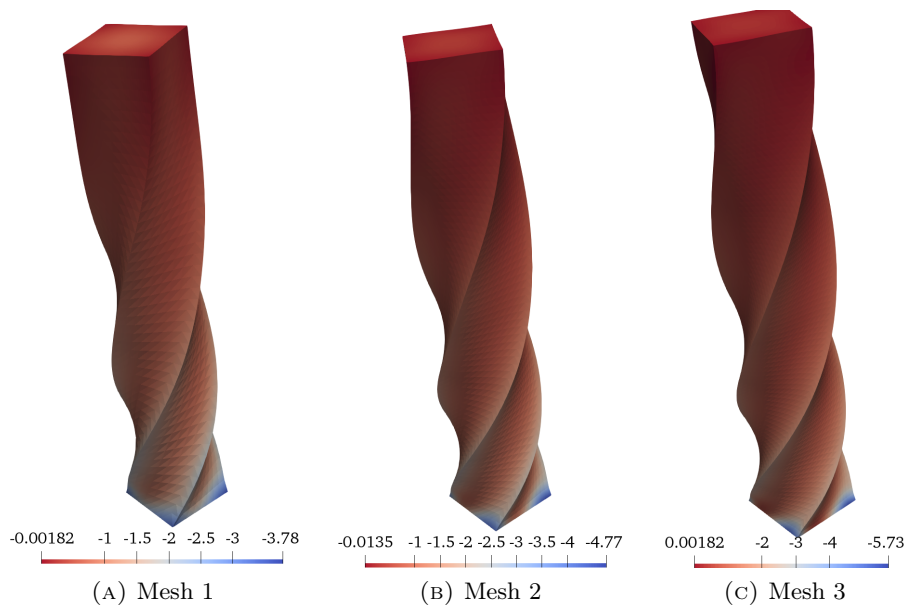


FIGURE 13. Twisting column. Deformation and pressure field (MPa) for  $\delta t = 0.001$  s at  $t = 0.3$  s with the OSS stabilization technique.

With regard to the time step, we can observe that Figures 11 and 13 are able to locate the maximum and minimum values of the pressure in the more stressed areas, in this case, near to the clamped boundary. It is interesting to observe that the mixed formulation proposed here produces a smooth and accurate pressure field for the fully incompressible case. Let

we also remark that for coarse meshes, we observe a spatial error which is propagated along time causing the difference in the deformation that we can appreciate in Figures 12 and 13. Clearly, our stabilized mixed implementation produces locking-free solutions and it does not exhibit non-physical pressure fluctuations thanks to both the application of BDF2, a high-frequency dissipation time integrator, and the application of VMS stabilization technique, which include sufficient numerical stabilization to the problem.

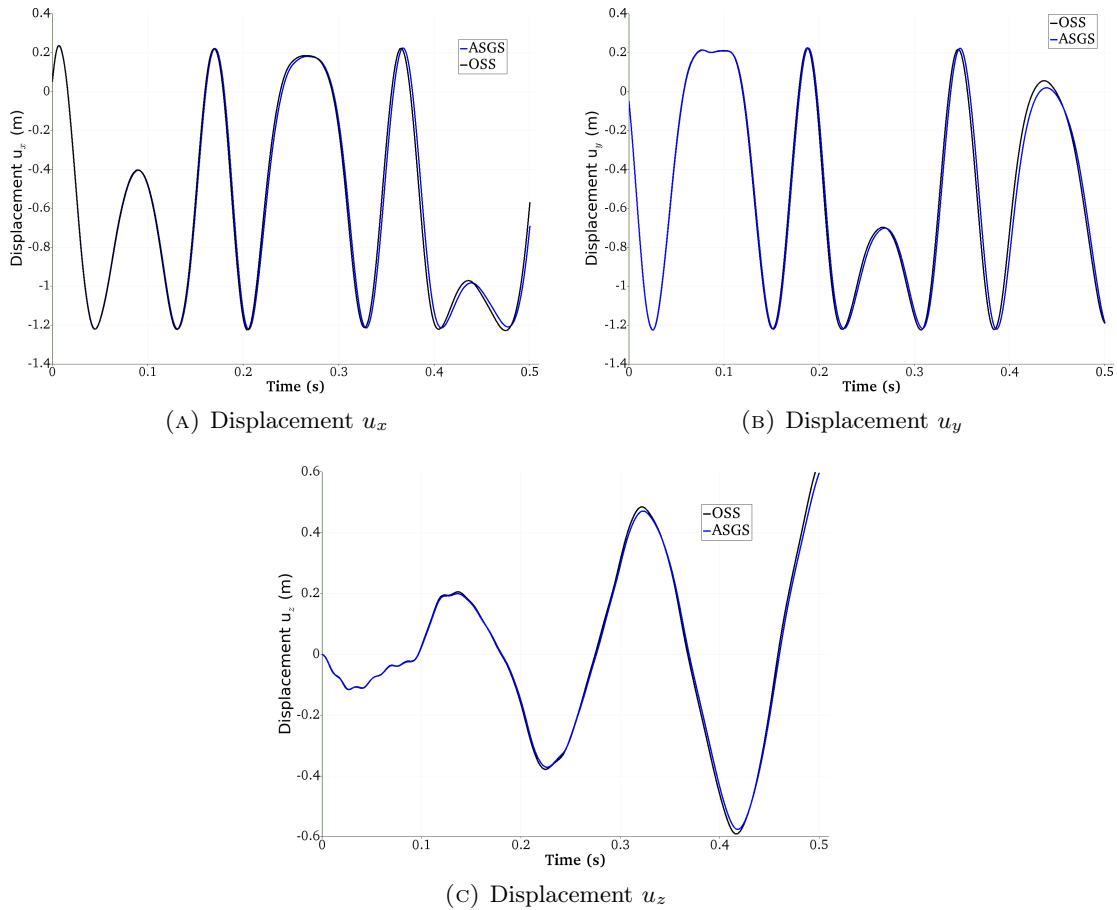


FIGURE 14. Twisting column. Displacement field at point A.

In Figure 14, we consider a comparison of the ASGS and OSS stabilization techniques of the mixed formulation for Mesh 3 and  $\delta t = 0.001$  s. Both stabilizations seem to closely track each other, also considering the fact that the OSS technique is more dependent of the time step size due to the approximation in the computation of the projection onto the finite element space. According to the solutions presented in [27], the displacement field is correctly captured with both stabilization methods.

To end up this numerical simulation, Figure 15 shows the evolution of the deformation of the twisting column along time up to  $T = 0.5$  s for Mesh 3 and with  $\delta t = 0.001$  s and using the ASGS stabilization method. It is easy to observe the well-reproduced evolution of the deformation of the column. Taking into account that this example is considered very challenging due to the extreme nonlinear deformations and huge number of pressure modes that appear, we remark the robustness and applicability of our stabilized mixed formulation.

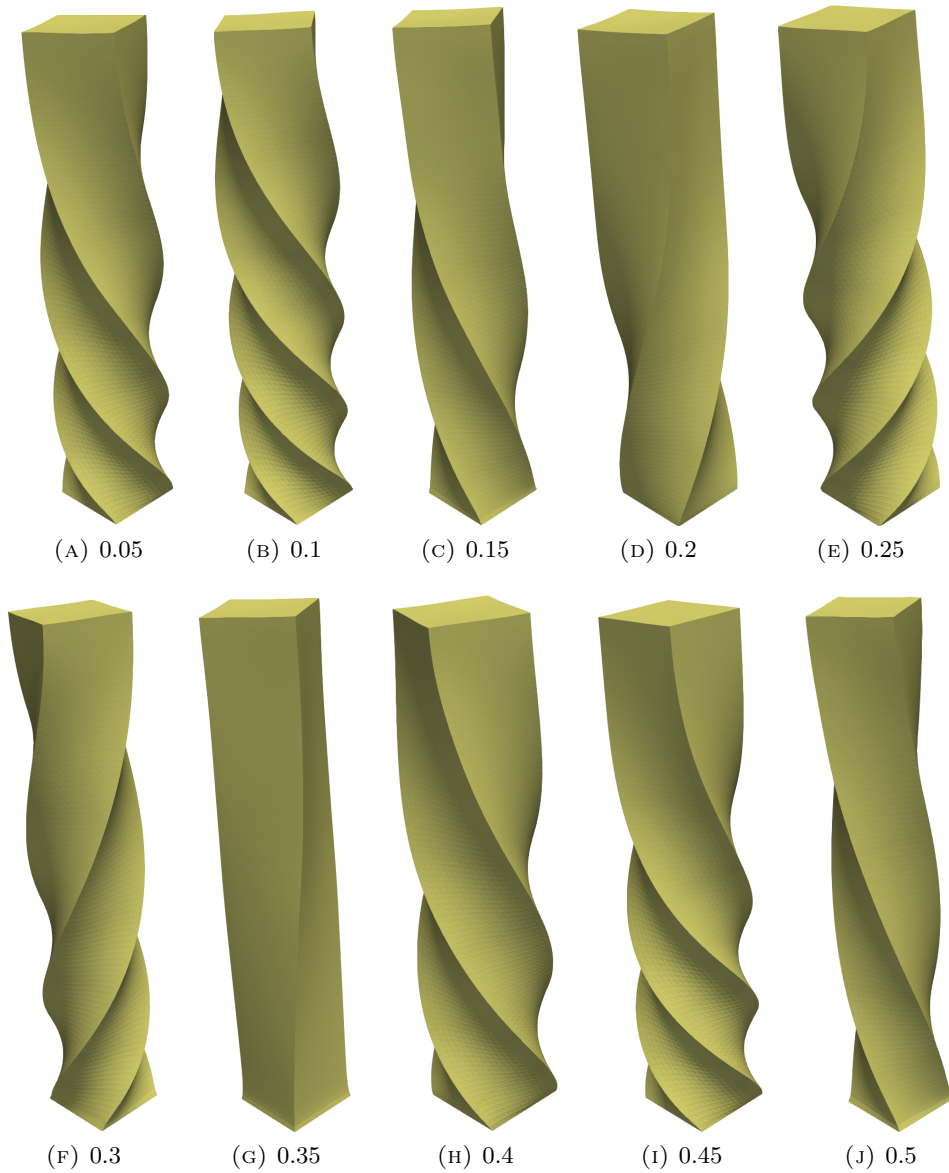


FIGURE 15. Twisting column. Deformation along time (in s).

## 5. CONCLUSIONS

In this paper we have described a new simple stabilized finite element method for the study of solid dynamics when considering nearly and fully incompressible materials. The point of departure is the splitting of the Cauchy stress tensor into deviatoric and spherical components, which then translates into a splitting of the second Piola-Kirchhoff stress tensor.

Regarding to the constitutive law, we have presented a formulation which works properly for any hyperelastic material model in which the strain energy function can be decomposed in deviatoric and volumetric parts, the latter in terms of the bulk modulus,  $\kappa$ . We have taken advantage of this decomposition to obtain a constitutive law for the pressure from the volumetric part. This law is formulated properly to obtain a simple way to impose the incompressibility of the material automatically. The resulting equation has been added

to the momentum equation to obtain a monolithic system of equations for the displacement/pressure pair.

With regard to the time integration scheme, we have shown that although any time integrator can be applied, implicit high-frequency dissipation time integration schemes are more suitable. To avoid pressure fluctuations of our solution along time, high-frequency dissipation schemes are recommended.

In Section 3 we have proposed a residual-based stabilization technique based on the decomposition of the unknowns into finite element scales and subgrid scales. Unlike the standard VMS stabilization technique, we have proposed to use the OSS formulation. In this approach the subgrid scale space is supposed to be perpendicular to the finite element one. As shown in Section 4, this stabilization exhibits better accuracy than the classical ASGS method for a fixed mesh. A key point is the way we have selected the stabilization parameters, where we have decided to give a closed-form expression based on previous works. We have shown also that the approximation of considering the subgrid scales to be modelled as bubble functions does not pollute the solution. Likewise, for the examples we have considered, we have been able to assume quasi-static subscales, although dynamic subscales might need to be considered if very small time step sizes are used.

Concerning the computational cost of the method, even if we have not shown this, we have observed that the methods proposed display (almost) quadratic non-linear convergence, as it is expected from the implementation of a Newton-Raphson iterative procedure. The number of unknowns is only increased by one per each node with respect to the classical irreducible displacement-based formulation, which is the minimum to be able to enforce incompressibility.

#### ACKNOWLEDGEMENTS

Inocencio Castañar gratefully acknowledges the support received from the Agència de Gestió d’Ajut i de Recerca through the predoctoral FI grant 2019-FI-B-00649. J. Baiges gratefully acknowledges the support of the Spanish Government through the Ramón y Cajal grant RYC-2015-17367. R. Codina gratefully acknowledges the support received through the ICREA Acadèmia Research Program of the Catalan Government. This work was partially funded through the TOP-FSI: RTI2018-098276-B-I00 project of the Spanish Government.

#### REFERENCES

- [1] G. A. Holzapfel. *Nonlinear solid mechanics. A continuum approach for engineering*. Wiley, 2000.
- [2] G. A. Holzapfel. Biomechanics of soft tissue. *The Handbook of Materials Behavior*, 3:1049–1063, 2001.
- [3] T. Belytschko, W. K. Liu, and B. Moran. *Nonlinear Finite Elements for Continua and Structures*. Wiley, 2001.
- [4] T. J. R. Hughes. *The Finite Element Method: Linear Static and Dynamic Finite Element Analysis*. Prentice-Hall, Englewood Cliffs, New Jersey, 1987.
- [5] I. Babuška. Error-bounds for finite element method. *Numerische Mathematik*, 16(4):322–333, 1971.
- [6] D. S. Malkus and T. J. R. Hughes. Mixed finite element methods - Reduced and selective integration techniques: A unification of concepts. *Computer Methods in Applied Mechanics and Engineering*, 15:63–81, 1978.
- [7] T. J. R. Hughes, L. P. Franca, and M. Balestra. A new finite element formulation for computational fluid dynamics: V. Circumventing the babuška-brezzi condition: a stable Petrov-Galerkin formulation of the stokes problem accommodating equal-order interpolations. *Computer Methods in Applied Mechanics and Engineering*, 59:85–99, 1986.
- [8] R. Codina. A stabilized finite element method for generalized stationary incompressible flows. *Computer Methods in Applied Mechanics and Engineering*, 190:2681–2706, 2001.
- [9] L. P. Franca, T. J. R. Hughes, A. F. D. Loula, and I. Miranda. A new family of stable elements for nearly incompressible elasticity based on a mixed Petrov-Galerkin finite element formulation. *Numerische Mathematik*, 53(1–2):123–141, 1988.

- [10] M. Chiumenti, Q. Valverde, C.A. de Saracibar, and M. Cervera. A stabilized formulation for incompressible elasticity using linear displacement and pressure interpolations. *Computer Methods in Applied Mechanics and Engineering*, 191:1095–1116, 2002.
- [11] M. Cervera, M. Chiumenti, and R. Codina. Mixed stabilized finite element methods in nonlinear solid mechanics. Part I: Formulation. *Computer Methods in Applied Mechanics and Engineering*, 199(37–40):2559–2570, 2010.
- [12] M. Cervera, M. Chiumenti, and R. Codina. Mixed stabilized finite element methods in nonlinear solid mechanics. Part II: Strain localization. *Computer Methods in Applied Mechanics and Engineering*, 199(37–40):2571–2589, 2010.
- [13] R. Codina. Stabilized finite element approximation of transient incompressible flows using orthogonal subscales. *Computer Methods in Applied Mechanics and Engineering*, 191:4295–4321, 2002.
- [14] R. Codina, J. M. González-Ondina, G. Díaz-Hernández, and J. Príncipe. Finite element approximation of the modified Boussinesq equations using a stabilized formulation. *International Journal For Numerical Methods in Engineering*, 57:1249–1268, 2008.
- [15] T. J. R. Hughes, G. R. Feijóo, L. Mazzei, and J. Quincy. The variational multiscale method - a paradigm for computational mechanics. *Computer Methods in Applied Mechanics and Engineering*, 166:3–24, 1998.
- [16] M. Chiumenti, M. Cervera, and R. Codina. A mixed three-field FE formulation for stress accurate analysis including the incompressible limit. *Computer Methods in Applied Mechanics and Engineering*, 283:1095–1116, 2015.
- [17] J. Bonet and A. J. Burton. A simple average nodal pressure tetrahedral element for incompressible and nearly incompressible dynamic explicit applications. *Computer Methods in Applied Mechanics and Engineering*, 1(4):437–449, 1998.
- [18] C. H. Lee, A. J. Gil, and J. Bonet. Development of a cell centred upwind finite volume algorithm for a new conservation law formulation in structural dynamics. *Computers and Structures*, 118:13–38, 2013.
- [19] M. Aguirre, A. J. Gil, J. Bonet, and A. Arranz-Carreño. A vertex centred finite volume Jameson-Schmidt-Turkel (JST) algorithm for a mixed conservation formulation in solid dynamics. *Journal of Computational Physics*, 259:672–699, 2014.
- [20] C. H. Lee, J. Haider, A. J. Gil, and J. Bonet. A first-order hyperbolic framework for large strain computational solid dynamics. An upwind cell centred Total Lagrangian scheme. *International Journal for Numerical Methods in Engineering*, 109:407–456, 2017.
- [21] C.H. Lee, A. J. Gil, and J. Bonet. Development of a stabilised Petrov-Galerkin formulation for linear tetrahedral elements in compressible, nearly incompressible and truly incompressible fast dynamics. *Computer Methods in Applied Mechanics and Engineering*, 268:40–64, 2014.
- [22] C.H. Lee, A. J. Gil, J. Bonet, and M. Aguirre. A stabilised Petrov-Galerkin formulation for linear tetrahedral elements in compressible, nearly incompressible and truly incompressible fast dynamics. *Computer Methods in Applied Mechanics and Engineering*, 276:659–690, 2014.
- [23] M. Aguirre, A. J. Gil, J. Bonet, and C. H. Lee. An upwind vertex centred finite volume solver for Lagrangian solid dynamics. *Journal of Computational Physics*, 300:387–422, 2015.
- [24] J. Bonet, A. J. Gil, C. H. Lee, M. Aguirre, and R. Ortigosa. A first order hyperbolic framework for large strain computational solid dynamics. Part I : Total Lagrangian isothermal elasticity. *Computer Methods in Applied Mechanics and Engineering*, 283:689–732, 2015.
- [25] A. J. Gil, C. H. Lee, J. Bonet, and R. Ortigosa. A first order hyperbolic framework for large strain computational solid dynamics. Part II : Total Lagrangian compressible, nearly incompressible and truly incompressible elasticity. *Computer Methods in Applied Mechanics and Engineering*, 300:146–181, 2016.
- [26] O. I. Hassan, A. Ghavamian, C. H. Lee, A. J. Gil, J. Bonet, and F. Auricchio. An upwind vertex centred finite volume algorithm for nearly and truly incompressible explicit fast solid dynamic applications: Total and Updated Lagrangian formulations. *Journal of Computational Physics : X*, 3:100025, 2019.
- [27] G. Scovazzi, B. Carnes, X. Zeng, and S. Rossi. A simple, stable, and accurate linear tetrahedral finite element for transient, nearly, and fully incompressible solid dynamics: a dynamic variational multiscale approach. *International Journal For Numerical Methods in Engineering*, 106:799–839, 2016.
- [28] S. Rossi, N. Abboud, and G. Scovazzi. Implicit finite incompressible elastodynamics with linear finite elements: A stabilized method in rate form. *Computer Methods in Applied Mechanics and Engineering*, 311:208–249, 2016.
- [29] C. Sansour. On the physical assumptions underlying the volumetric-isochoric split and the case of anisotropy. *European Journal of Mechanics A/Solids*, 27:28–39, 2008.
- [30] J. Bonet and R.D. Wood. *Nonlinear Continuum mechanics for finite element analysis*. Cambridge University Press, 1997.

- [31] C. O. Horgan and J. G. Murphy. On the volumetric part of strain-energy functions used in the constitutive modeling of slightly compressible solid rubbers. *International Journal of Solids and Structures*, 46:3028–3085, 2009.
- [32] J.C. Simo, R.L. Taylor, and K.S. Pister. Variational and projection methods for the volume constraint in finite deformation elasto-plasticity. *Computer Methods in Applied Mechanics and Engineering*, 51(1–3):177–208, 1985.
- [33] C. Miehe. Aspects of the formulation and finite element implementation of large strain isotropic elasticity. *International Journal for Numerical Methods in Engineering*, 12:1981–2004, 1994.
- [34] C. H. Liu, G. Hofstetter, and H. A. Mang. 3D finite element analysis of rubber-like materials at finite strains. *Engineering Computations*, 11(2):111–128, 1994.
- [35] R. Codina, S. Badia, J. Baiges, and J. Principe. *Variational Multiscale Methods in Computational Fluid Dynamics*, in Encyclopedia of Computational Mechanics, pages 1–28. John Wiley & Sons Ltd., 2017.
- [36] S. Badia and R. Codina. Unified stabilized finite element formulations for the Stokes and the Darcy problems. *SIAM Journal on Numerical Analysis*, 47(3):1971–2000, 2009.
- [37] R. Codina. Stabilization of incompressibility and convection through orthogonal sub-scales in finite element methods. *Computer Methods in Applied Mechanics and Engineering*, 190:1579–1599, 2000.
- [38] H. A. Van der Vorst. Bi-CGSTAB: A fast and smoothly converging variant of Bi-CG for the solution of nonsymmetric linear systems. *SIAM, Journal of Scientific and Statistical Computing*, 13(2):631 – 644, 1992.
- [39] S. Balay, S. Abhyankar, M. F. Adams, J. Brown, P. Brune, K. Buschelman, L. Dalcin, V. Eijkhout, W. D. Gropp, D. Kaushik, M. G. Knepley, D. A. May, L. Curfman McInnes, R. T. Mills, T. Munson, K. Rupp, P. Sanan, B. F. Smith, S. Zampini, H. Zhang, and H. Zhang. PETSc Web page, <http://www.mcs.anl.gov/petsc>, 2015.
- [40] J. Chung and G. M. Hulbert. A Time Integration Algorithm for Structural Dynamics with improved numerical dissipation: The generalized- $\alpha$  method. *Journal of Applied Mechanics*, 60(2):371 – 375, 1993.
- [41] T. Elguedj, Y. Bazilevs, V. M. Calo, and T. J. R. Hughes.  $\bar{B}$  and  $\bar{F}$  projection methods for nearly incompressible linear and nonlinear elasticity and plasticity using higher-order NURBS elements. *Computer Methods in Applied Mechanics and Engineering*, 197:2732–2762, 2008.
- [42] B. Müller, G. Starke, A. Schwarz, and J. Schröder. A first-order system least squares method for hyperelasticity. *Society for Industrial and Applied Mathematics*, 36(5):B795–B816, 2014.
- [43] J. Baiges and R. Codina. Variational multiscale error estimators for solid mechanics adaptive simulations: an orthogonal subgrid scale approach. *Computer Methods in Applied Mechanics and Engineering*, 325:37–55, 2017.
- [44] F. Auricchio, L. B. da Veiga, C. Lovadina, A. Reali, R. L. Taylor, and P. Wriggers. Approximation of incompressible large deformation elastic problems: some unresolved issues. *Computational Mechanics*, 52(5):1153–1167, 2013.
- [45] J. Schröder, N. Viebahn, P. Wriggers, F. Auricchio, and K. Steeger. On the stability analysis of hyperelastic boundary value problems using three- and two-field mixed finite element formulations. *Computational Mechanics*, 60:479–492, 2017.
- [46] X. Oliver and C. A. de Saracibar. *Continuum Mechanics for Engineers. Theory and Problems, 2nd edition*. 2017.
- [47] E. Boman, K. Devine, L. A. Fisk, R. Heaphy, B. Hendrickson, V. Leung, C. Vaughan, U. Catalyurek, D. Bozdog, and W. Mitchell. Zoltan home page, <http://www.cs.sandia.gov/zoltan>. *Sandia National Laboratories*, 1999.
- [48] W. Schroeder, K. Martin, and B. Lorensen. *The Visualization Toolkit (4th ed.)*. Kitware, 2006.